

EFFECT ON SHEAR BEHAVIOUR OF STAINLESS STEEL LIPPED CHANNEL BEAMS WITH PERFORATION

Dr.K.Rekha¹, P.R.Harshini^{2*}

¹*Assistant Professor, ²PG scholar*

Department of Civil Engineering, Government College of Technology,

Coimbatore, India - 641013

Corresponding author's email [E mail: harshini271002@gmail.com]

Co author's email [E mail: krekha@gct.ac.in]

Acknowledgement

The authors acknowledge the support and cooperation of the technical staff and colleagues who assisted at various stages of this research. The authors also appreciate the constructive comments and suggestions provided by the reviewers, which helped to improve the quality of this manuscript.

This research received no specific grant from any funding agency in the public, commercial, or not-for-profit sectors and was carried out using the facilities available at the authors' institution.

EFFECT ON SHEAR BEHAVIOUR OF STAINLESS STEEL LIPPED CHANNEL BEAMS WITH PERFORATION

ABSTRACT

Stainless steel is widely used in modern construction due to its high strength, corrosion resistance, and durability and are commonly used as purlins and framing members. Their shear behaviour, especially with web perforations, is complex due to nonlinear stress-strain characteristics, local buckling, and strain hardening. This project investigates the shear behaviour of cold-formed stainless steel (CFSS) lipped channel beams (LCBs) with circular web perforations through numerical and theoretical studies. A detailed literature review revealed that existing standards such as Direct Strength Method and Eurocode 3 often underestimate shear capacity, particularly for perforated sections. Section properties and buckling modes were determined using CUFSM Software, while detailed Finite Element (FE) models were developed in ABAQUS to analyse shear behaviour. A total of 100 models were analysed by varying web thickness (1.5, 2, 2.5, 3 mm), web depth, and perforation ratios (0.2, 0.4, 0.6, 0.8). Among different perforation geometries (Circle, Diamond, Square), circular openings showed superior shear performance. The results indicated that shear capacity decreased with increasing perforations. Theoretical analysis using the Effective Width Method (EWM) and Direct Strength Method (DSM) highlighted limitations in existing design equations. Modified DSM and Eurocode formulations were then proposed by introducing a shear-capacity reduction factor (q_s) and equivalent web thickness (t_{eq}) to better represent perforation effects.

Key words: Stainless Steel, Lipped Channel Beam, Shear Capacity, Web Perforation, Direct Strength Method, Euro Code.

1. INTRODUCTION

Steel structural systems have become an essential part of modern construction due to their high structural efficiency, faster erection, and adaptability in various environments. In recent years, stainless steel has emerged as a superior alternative to conventional carbon steel, particularly for structures requiring improved durability, corrosion resistance, and reduced maintenance throughout their service life. Its inherent mechanical properties such as high strength, ductility, strain-hardening capability, and excellent resistance to aggressive environments make it highly suitable for long-span and lightweight structural applications. Cold-formed stainless steel (CFSS) members, manufactured by forming thin steel sheets at room temperature, are gaining substantial attention in the construction industry. Among these, lipped channel beams are widely adopted for secondary load-bearing components such as purlins, girts, floor joists, wall studs, and modular framing systems which is depicted in Figure 1 . Their high strength-to-weight ratio and enhanced local buckling resistance make them an efficient solution for lightweight structural systems. However, the thin-walled nature of these sections causes complex failure modes such as local, distortional, and lateral-torsional buckling under different loading conditions, necessitating careful design considerations.

Furthermore, the integration of web perforations has become common in modern design practices to facilitate services such as electrical conduits, ventilation ducts, and plumbing systems through the beam web which is represented in Figure 1 . Although these openings increase functional efficiency, they significantly influence shear behaviour by reducing effective web area and altering stress distribution. The presence of perforations may lead to premature shear buckling and reduced load-carrying capacity if not properly designed and assessed. With the increasing adoption of stainless steel in coastal infrastructure, industrial facilities, and renewable energy structures, understanding the shear performance of perforated CFSS lipped channel beams becomes essential for establishing safe and economical design solutions. Existing design standards such as Eurocode 3 and AS/NZS provisions provide limited guidance for stainless steel members with web openings, and their prediction accuracy for shear capacity remains uncertain due to the nonlinear material response and prominent post-buckling strength associated with stainless steel.



Figure 1 Stainless Steel Lipped Channel Beam in Practical Construction

Vadivelu (2025)[1] examined perforated stainless steel RHS beams under flexure using experiments and FE analysis, showing that large perforations significantly reduce capacity and existing codes are inadequate, leading to proposed design reduction factors. Huangfu et al. (2025)[2] investigated folded-flange, V-stiffened C-shaped stainless steel beams through bending tests and FE models, finding that higher web slenderness improves shear capacity while edge stiffeners have limited effect. Jiao (2025)[3] investigated the shear behavior of stainless steel I-section beams using experiments and FE analysis, showing reduced shear capacity with increasing web slenderness, conservative code predictions, and proposing refined design recommendations considering post-buckling effects. Ivković et al. (2024)[4] applied artificial neural networks to accurately predict mechanical properties of AISI 304 and 316 stainless steels from chemical composition, achieving errors within 5–10%.

Perampalam et al. (2024) [5] investigated cold-formed stainless steel lipped channel sections with circular web holes using experiments and FE analysis, showing significant shear strength reduction at high perforation ratios, inadequacy of Eurocode 3, and proposing an equivalent web thickness method for improved design. Simwanda et al. (2024) [6] developed ML models (XGBoost, CatBoost) based on extensive FE data to predict bending capacity of perforated CFS beams with very high accuracy ($R^2 \approx 99.9\%$), demonstrating the superiority of data-driven approaches over traditional DSM methods. Vu et al. (2024) [7] provided a comprehensive review of perforated cold-formed steel members, highlighting the influence of web hole geometry on buckling behavior, limitations of existing design methods, and the need for refined predictive and design guidance. Amani et al. (2023) [8], Real et al. (2023) [9], and Zhou et al. (2023) [10] investigated stainless steel girders with corrugated and perforated webs, showing enhanced shear stiffness due to corrugation, significant effects of material nonlinearity and web slenderness, and notable shear capacity reductions governed by

perforation geometry. Gatheeshgar et al. (2023) [11] and Yousefi et al. (2023) [12] critically assessed Eurocode shear and bearing provisions for stainless steel members, identifying major discrepancies for perforated sections and proposing refined design recommendations. Degtyarev & Tsavdaridis (2022) [13] and Li et al. (2022) [14] demonstrated that machine learning and FE-based approaches outperform traditional codes in predicting buckling and shear capacity of cellular and perforated girders. Mangattil & Divya (2022) [15] further showed that perforation shape, size, and layout strongly influence shear capacity of lean duplex stainless steel RHS beams, with existing standards proving inadequate and requiring reduction factors for safe design.

Dissanayake et al. (2021, 2020) [16, 23] and Chen et al. (2020) [22] investigated bending–shear interaction and shear behavior of cold-formed and plate-type stainless steel members using experiments and FE analysis, showing significant post-buckling and strain-hardening effects and that existing Eurocode/DSM interaction rules are often conservative or unsafe. Ishqy et al. (2021) [17], Yousefi et al. (2021) [18], and De’nan et al. (2021) [19] focused on stainless steel channel beams with web openings, demonstrating substantial shear capacity reductions due to perforations, strong stress concentrations, and the need for perforation-specific reduction factors. Kweon (2021) [20] and Mohammed & Cashell (2021) [21] improved material and column design accuracy by developing reliable stress–strain models and applying the Continuous Strength Method to account for strain hardening and elevated temperature effects. Laím et al. (2020) [24] investigated torsional and flexural behavior of cold-formed stainless steel channels using experiments and FE analysis, identifying strong effects of web slenderness and flange width and proposing improved torsion design rules due to code discrepancies. Keerthan et al. (2019) [25] and Roy & Lim (2019) [26] examined perforated and built-up stainless steel channel members through FE studies, showing significant strength reductions due to openings or slenderness, inconsistencies in existing codes, and proposing reduction factors and joint design recommendations. Chen et al. (2018) [27] studied shear buckling of stiffened stainless steel plate girders, demonstrating enhanced post-buckling capacity due to strain hardening and the effectiveness of transverse stiffeners, emphasizing the need for stainless-steel-specific design provisions.

Divya and Keerthan (2018) [28], Pham et al. (2016) [33], and Lawson et al. (2015) [36] investigated cold-formed steel members with perforated webs using FE and experimental studies, demonstrating significant shear capacity reductions, altered buckling modes, and the inadequacy of existing DSM and code-based design rules for perforated sections. Nilakanmani & Anbarasu (2018) [30] and Arrayago et al. (2015) [34] advanced stainless steel

modelling by developing validated nonlinear FE and material stress–strain models, improving prediction of strength, stiffness, and post-buckling behaviour across different stainless steel grades. Tiwari et al. (2018) [29] demonstrated that combining bottom ash with coir fibers significantly improves the strength and durability of expansive soils, supporting sustainable and eco-friendly geotechnical construction. Baddoo and Francis (2014) [37] and Cashell and Baddoo (2014) [38] reviewed the development of stainless steel design rules and applications, highlighting nonlinear material behavior, buckling, durability, and the structural potential of ferritic stainless steels. Keerthan & Divya (2008) [39] investigated hollow flange LiteSteel beams in shear, showing notable post-buckling strength and identifying the conservatism of AS/NZS 4600 shear provisions for thin-web sections. The FE models effectively captured local deformations, stress redistribution, and post-buckling behaviour, with parametric studies considering flange width, web slenderness, and beam length, leading to the proposal of refined shear design equations accounting for post-buckling strength.

Overall, the reviewed studies indicate that cold-formed stainless steel lipped channel beams retain significant load-carrying capacity after shear buckling due to strain hardening; however, the presence of web openings causes notable strength reduction because of material loss and stress concentration effects. Although extensive experimental and FE research exists, current design standards such as Eurocode 3 [40] and AS/NZS [31] do not adequately capture these behaviours and often provide overly conservative predictions, highlighting the need for further research to develop reliable DSM-based design rules and reduction factors for perforated stainless steel lipped channel beams to ensure both safety and material efficiency in practice.

2. FINITE ELEMENT MODELLING

Finite element modelling of the stainless steel lipped channel beams (LCBs) with web openings was carried out using ABAQUS[41] to accurately capture their shear behaviour, buckling response, and ultimate failure mechanisms under loading. The geometric modelling began by creating deformable shell parts using the centre-line dimensions of the lipped channel section along with the actual plate thickness, ensuring precise representation of the thin-walled geometry. Each section was generated using the shell extrusion method, enabling the formation of long prismatic members commonly used in structural applications. Material properties were defined in the Property module, where elastic constants such as Young's modulus (210000 N/mm^2), Poisson's ratio (0.3), and density ($7.85 \times 10^{-6}\text{ N/mm}^3$) were specified for linear analysis, while nonlinear stress–strain behaviour was incorporated through true stress–plastic

strain curves derived from tensile coupon tests shown in Figure 2. Coupon tests, conducted on stainless steel grade 304 with thicknesses of 2.5 mm and 3.0 mm, provided yield strength, ultimate tensile strength, elongation, and breaking strength, which were essential for capturing the strain-hardening behaviour in nonlinear FEA. The engineering stress–strain data from the tests were converted into true stress and true strain values to reflect the actual material response under large deformation, enabling accurate modelling of yielding and post-yield phenomena that strongly influence shear capacity and buckling behaviour depicted in Figure 3.



Figure 2 Coupon testing of Stainless steel Specimen

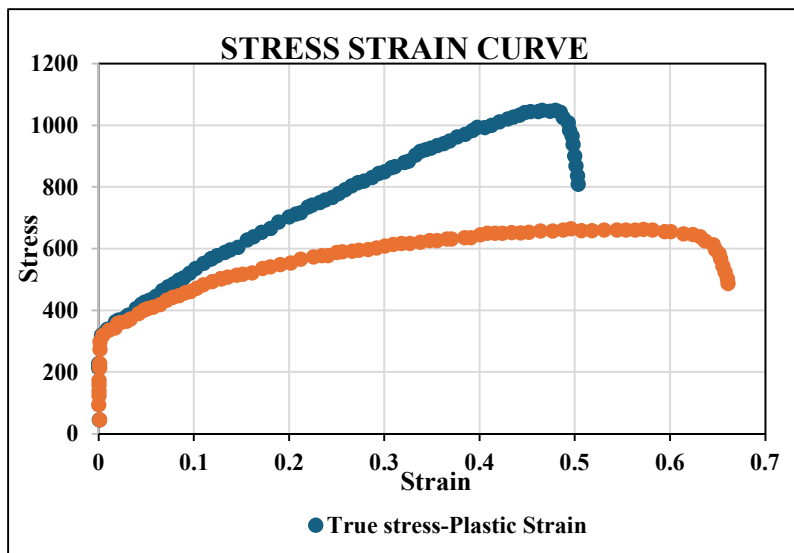


Figure 3 True stress and Plastic Strain from Testing of specimen

Table 1 In the Assembly module, the lipped channel part was instanced and positioned in the global coordinate system for further analysis. To simulate realistic experimental boundary

conditions, rigid web-side plates were modelled at the supports and loading points using R3D4 rigid elements. These plates ensured that the applied loads and reaction forces were transferred through the shear centre of the section, preventing unintended torsional effects. The shear centre value was obtained from CUFSM (Constrained and Unconstrained Finite Strip Method) software[411]. Reference points (RPs) were created and linked to these rigid plates through rigid body constraints, enabling controlled application of loads and enforcement of boundary conditions as provided in [5]. Translational and rotational degrees of freedom were assigned appropriately: supports provided restraint against vertical and lateral movement while allowing rotation, the mid-span loading point was free in vertical translation to permit deflection, and angle straps were modelled through equivalent boundary conditions rather than explicit modelling, ensuring computational efficiency without compromising behavioural accuracy as shown in Table 1 and Figure 4 .

Boundary Condition for Support and Straps[5]

Left and right supports	Mid-span loading
$U_x = \text{restrained} ; \theta_x \text{ free}$ $U_y = \text{restrained} ; \theta_y = \text{free}$ $U_z = \text{free} ; \theta_z = \text{restrained}$	$U_x = \text{restrained} ; \theta_x = \text{free} ; U_y = \text{free} ; \theta_y = \text{free}$ $U_z = \text{restrained} ; \theta_z = \text{restrained}$
Strap location	$U_x = \text{restrained} ; \theta_x = \text{free}$ $U_y = \text{free} ; \theta_y = \text{free}$ $U_z = \text{free} ; \theta_z = \text{restrained}$

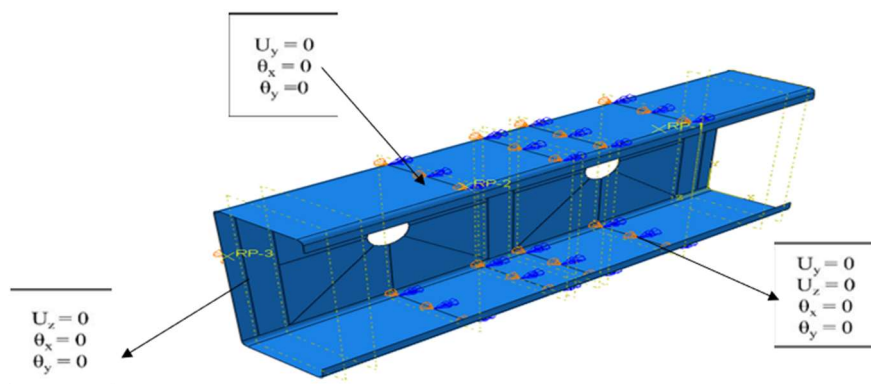


Figure 4 Boundary Condition for Straps and Support

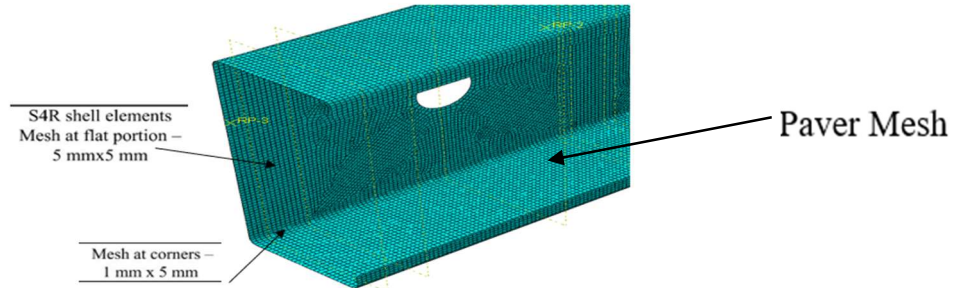


Figure 5 Mesh Applied to SSLCB

Meshing was performed using S4R four-node quadrilateral shell elements with reduced integration, which are well-suited for thin-walled structural members subjected to complex buckling and post-buckling behaviour[5]. A paver meshing technique was employed to generate smooth, high-quality meshes across the section, while mesh refinement was applied around perforations and corner regions to accurately capture high stress gradients and localized deformation patterns. Mesh sizes of 1×5 mm were used along the corners and webs near openings, and 5×5 mm elements were used along the flat portions to maintain computational efficiency without sacrificing accuracy which is depicted in Figure 5.

Geometric imperfections, which play a significant role in the buckling and post-buckling behaviour of thin-walled members, were incorporated through a linear eigenvalue buckling analysis. This analysis identified the most critical buckling modes, and the first eigenmode was scaled using a fabrication tolerance expression to generate the initial imperfect geometry for nonlinear analysis. This ensured realistic prediction of failure loads, as perfect geometry often leads to unconservative high buckling capacities. Following this, nonlinear analysis was performed using the arc-length-based Riks method, which is capable of tracing unstable equilibrium paths and capturing snap-through or snap-back behaviour common in thin-walled sections. The initial geometric imperfections were taken as the fabrication tolerance limit of $\omega = 0.023(\frac{\sigma_{0.23}}{\sigma_{cr}}) \times t$. The nonlinear solver accounted for large deformations, geometric nonlinearity, and material plasticity, thereby providing a realistic simulation of shear buckling, local distortions around perforations, and eventual collapse.

The complete analysis procedure involved creating the section based on centre-line dimensions, assigning both elastic and nonlinear material properties, assembling the part, generating a refined mesh, defining boundary conditions and rigid constraints, and applying a

unit transverse load for eigenvalue buckling analysis. The lowest buckling mode was then used to introduce initial imperfections into the model for subsequent nonlinear analysis. Load–deflection curves obtained from the nonlinear analysis allowed determination of critical buckling loads, post-buckling response, and ultimate shear capacity. Linear analysis provided idealized buckling shapes, whereas nonlinear analysis captured actual behaviour including local yielding, large deflections, buckling–post-buckling interactions, and shear failure patterns.

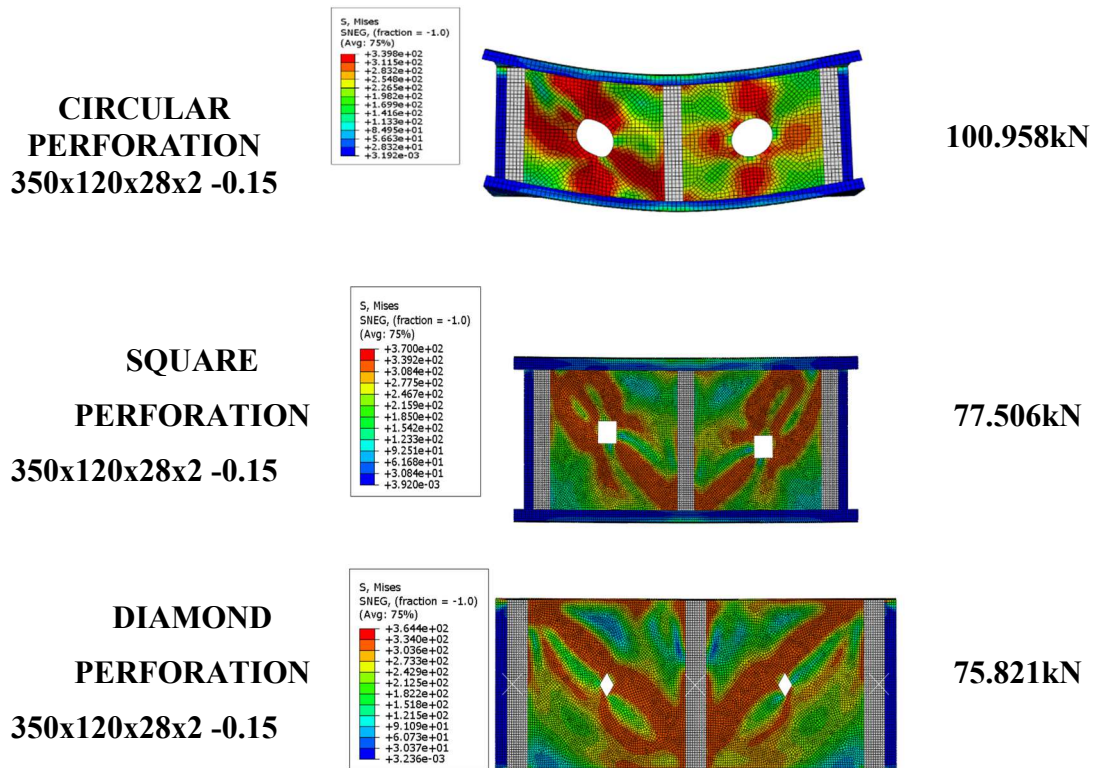
3. SELECTION OF SECTIONS AND PARAMETRIC STUDY

A detailed parametric study was conducted to examine how variations in section geometry and web perforation affect the shear behaviour of cold-formed stainless steel lipped channel beams. Five channel sections were selected based on the width-to-thickness limits specified in EN 1993-1-3[40], ensuring that the chosen profiles represent practical and structurally efficient cold-formed members. Each section was analysed with four different material thicknesses ranging from 1.5 mm to 3.0 mm, and circular web openings were introduced using perforation ratios of 0.2, 0.4, 0.6 and 0.8. This resulted in a total of 100 finite element models as tabulated in Table 2 . Circular perforations were chosen for the full study because preliminary comparisons indicated that they produce a more uniform stress distribution around the opening and retain higher shear capacity compared with square or diamond openings, which tend to develop high stress concentrations at their corners. All models were assigned stainless steel properties with a yield strength of 650 MPa, and nonlinear stress–strain behaviour was included to reflect the actual material response under shear and local buckling. The results of the study clearly showed that the ultimate shear capacity decreases as the perforation ratio increases, primarily due to the reduction in effective web area and the increased likelihood of shear-induced buckling near the opening. Sections with larger web depths and thicker plates consistently demonstrated higher shear strength, whereas slender sections were more vulnerable to premature local buckling when larger openings were present. Overall, the parametric investigation provides valuable insights into how web dimensions, thickness, and perforation size interact to govern the shear performance of perforated stainless steel lipped channel beams, and the findings contribute to the development of more reliable design recommendations for these members.

Table 2 Section for Parametric Study

Specimen ID	Thickness (mm)
LC-150x60x18	1.5,2,2.5,3
LC-200x65x20	1.5,2,2.5,3
LC-250x70x22	1.5,2,2.5,3
LC-300x75x25	1.5,2,2.5,3
LC-350x120x28	1.5,2,2.5,3

Table 3 Shear Behaviour for Different Perforation



The finite element analysis highlights the significant influence of perforation geometry on the shear behaviour of cold-formed steel lipped channel beams. Among the three configurations studied, beams with circular perforations demonstrated the highest shear capacity (100.958 kN), primarily due to their smooth boundary profile, which promotes uniform stress flow and minimizes localized stress concentrations as shown in Table 3. Conversely, square perforations resulted in a reduced capacity (77.506 kN), as the sharp corners intensified stress accumulation and accelerated the onset of shear buckling. The

diamond-shaped perforations exhibited the lowest strength (75.821 kN), attributed to the presence of acute angles that further amplify stress gradients within the web. Overall, the results clearly indicate that circular openings offer a more favourable structural response under shear, whereas square and diamond perforations compromise the shear performance due to geometric discontinuities.

4.THEORTICAL STUDY

The theoretical investigation in this study examines the applicability and limitations of the two major design approaches used for predicting the shear capacity of cold-formed stainless steel members—the Effective Width Method (EWM) and the Direct Strength Method (DSM). Although the EWM has been traditionally adopted for carbon steel sections, its use in stainless steel design is challenging because stainless steel exhibits a nonlinear stress-strain response, lacks a distinct yield point, and displays significant strain hardening. These material characteristics, combined with the presence of lips, stiffeners and web perforations, make the effective-width calculations increasingly complex and often lead to conservative or inconsistent predictions. The DSM provides a more rational alternative by determining member strength directly from elastic buckling behaviour without requiring effective-width reductions. It relates local, distortional and global buckling stresses to ultimate strengths and naturally incorporates the influence of geometric imperfections and post-buckling resistance, which are important for stainless steel behaviour. Previous studies support the use of DSM for stainless steel sections. Dissanayake et al. demonstrated that existing DSM shear equations underestimate the strength of stainless steel lipped channel beams because they do not fully capture strain hardening and the additional post-buckling capacity of the web, and they proposed modified DSM expressions to improve accuracy[5]. Similarly, Gatheeshgar et al. investigated stainless steel beams with circular web openings and introduced an equivalent web thickness to account for the reduction in shear-resisting area within the Eurocode design framework[11]. While these developments have improved the prediction of shear behaviour, the present study identifies that existing DSM and Eurocode provisions still do not adequately reflect the combined effects of perforation ratio, web slenderness and nonlinear material behaviour for the sections examined. Therefore, refined design expressions are developed in this research to enhance the reliability of shear capacity predictions for both perforated and non-perforated stainless steel lipped channel beams.

4.1 DSM DESIGN RULES FOR PURE SHEAR

4.1.1 DSM DESIGN RULES IN SHEAR WITHOUT TENSION FIELD ACTION

The nominal shear strength (V_n) of beams without holes in the web and without web stiffeners is determined from Appendix 1, section 1.2.2.2.1 of NAS-2012[31] as follows:

$$\lambda_v = \sqrt{\frac{V_y}{V_{cr}}} \quad (1)$$

Where, $V_y = 0.6 * f_y * A_w$

V_{cr} - elastic buckling force of the section (linear buckling force/2)

V_y – yield load of web

Nominal shear strength of beams without holes in the web and without web stiffeners is determined by

$$\text{for } \lambda_v \leq 0.815 : V_v = V_y \quad (2)$$

$$\text{for } 0.815 < \lambda_v \leq 1.227 : V_v = 0.815 \sqrt{V_{cr} V_y} \quad (3)$$

$$\text{for } \lambda_v > 1.227 : V_v = V_{cr} \quad (4)$$

$$v_{nl} = q_s \times v_v \quad (5)$$

Where q_s is Shear Capacity Reduction factor = v_{nl} / v_v

4.1.2 DESIGN RULES IN SHEAR WITH TENSION FIELD ACTION.

The nominal shear strength (V_n) of beams without holes in the web including tension field action is determined from Appendix 1,section 1.2.2.2.1 of NAS-2018 as follows:

$$V_v = \left[1 - 0.15 \left(\frac{V_{cr}}{V_y} \right)^{0.4} \right] \left(\frac{V_{cr}}{V_y} \right)^{0.4} V_y \quad (6)$$

$$v_{nl} = q_s \times v_v \quad (7)$$

$$V_{cr} = \frac{k_v \times \pi^2 \times E \times A_w}{12[1-\mu^2] \left(\frac{d_1}{t_w} \right)^2} \quad (8)$$

$$V_y = 0.6 \times A_w \times f_y \quad (9)$$

Where q_s is shear capacity reduction factor = v_{nl} / v_v

q_s for AS/NS 4600

$$q_s = \frac{c}{t} > 54$$

$$q_s = \frac{c}{54t} 5 \leq \frac{c}{t} \leq 54, C = \frac{d_1}{2} - \frac{d_{wh}}{2.83}$$

$$\frac{d_{wh}}{d_1} < 0.7, \frac{d_{wh}}{t_w} \leq 200, d_{wh} > 15\text{mm}, d_{wh} \leq 150\text{mm}$$

d_1 =clear height, d_{wh} =depth of web opening,t = thickness of web

4.1.3 PROPOSED DSM SHEAR DESIGN GUIDELINES BY DISSANAYAKE ET.AL - WITHOUT PERFORATION [5]

$$\lambda_v = \sqrt{\frac{V_y}{V_{cr}}}$$

Where, $V_y = 0.6 * f_y * A_w$

V_{cr} - elastic buckling force of the section (linear buckling force/2)

V_y – yield load of web

Nominal shear strength of beams without holes in the web and without web stiffeners is determined by

$$\text{for } \lambda_v \leq 0.122: \frac{Vv}{Vy} = 2 \quad (10)$$

$$\text{for } 0.122 < \lambda_v \leq 0.592: \frac{Vv}{Vy} = \frac{0.795}{\lambda^{0.439}} \quad (11)$$

$$\text{for } \lambda_v > 0.592: Vv = \left[1 - 0.15 \left(\frac{V_{cr}}{V_y} \right)^{0.4} \right] \left(\frac{V_{cr}}{V_y} \right)^{0.4} V_y \quad (12)$$

4.2 EN1993-1-4 SHEAR DESIGN RULES

The sectional shear resistance, $V_{b,Rd}$, of a stainless steel member is calculated as the sum of the web shear resistance ($V_{bw,Rd}$) and flange shear resistance ($V_{bf,Rd}$)[40]:

$$V_{b,Rd} = V_{bw,Rd} + V_{bf,Rd} \leq \frac{\eta f_{yw} h_w t_w}{\sqrt{3} \gamma_{M1}} \quad (14)$$

f_{yw} = design yield stress of the web (for stainless steel, typically the 0.2% proof stress)

h_w = clear depth of the web between flanges, t_w = web thickness , $\eta = 1.2$ is a recommended factor for stainless steel , γ_{M1} = partial safety factor

The **web shear resistance**, $V_{bw,Rd}$, is given by:

$$V_{bw,Rd} = \frac{\chi_w f_{yw} h_w t_w}{\sqrt{3} \gamma_{M1}} \quad (15)$$

where:

χ_w = web shear buckling reduction factor, which accounts for local buckling of the web. Values of χ_w for webs with rigid end-posts are provided in Figure 4.1 of EN 1993-1-4

	χ_w
$\bar{\lambda}_w \leq 0.65/\eta$	η
$0.65/\eta < \bar{\lambda}_w < 0.65$	$0.65/\bar{\lambda}_w$
$\bar{\lambda}_w \geq 0.65$	$1.56/(0.91 + \bar{\lambda}_w)$

$\bar{\lambda}_w$ = non-dimensional web slenderness, $\eta = 1.2$ for stainless steel

The web slenderness, $\bar{\lambda}_w$, is defined for webs with transverse stiffeners at supports and mid-span as:

$$\bar{\lambda}_w = \frac{h_w}{t_w} \frac{1}{37.4 \epsilon \sqrt{k_\tau}} \quad (16)$$

h_w = clear depth of the web between flanges, t_w = web thickness, ϵ = material factor, defined as:

$$\epsilon = \sqrt{\frac{235}{f_y}}$$

with f_y = yield stress of stainless steel (or 0.2% proof stress), and E = modulus of elasticity (typically 210,000 N/mm²).

k_τ = web shear buckling coefficient for plates with rigid transverse stiffeners and without longitudinal stiffeners, a = distance between transverse stiffeners given as:

$$k_\tau = 5.34 + 4.00 \left(\frac{a}{h_w}\right)^2 \text{ for } \frac{a}{h_w} \geq 1 \quad (17)$$

$$k_\tau = 4.00 + 5.34 \left(\frac{a}{h_w}\right)^2 \text{ for } \frac{a}{h_w} < 1 \quad (18)$$

These equations allow accurate determination of the web shear buckling reduction factor χ_w for stainless steel cold-formed members, taking into account material properties, web geometry, and stiffener spacing. The factor χ_w is then used in the web shear resistance equation:

$$V_{bw,Rd} = \frac{\chi_w f_{yw} h_w t_w}{\sqrt{3} \gamma_{M1}}$$

This ensures that the shear capacity of slender stainless steel webs is appropriately reduced to reflect potential local buckling while maintaining safety and code compliance.

The **flange shear resistance** give is calculated as

$$V_{bf,Rd} = \frac{b_f t_f}{2} \frac{f_{yf}}{c \gamma_{M1}} \left(1 - \left(\frac{M_{Ed}}{M_{f,Rd}}\right)^2\right)$$

b_f = flange width, t_f = flange thickness, f_{yf} = flange yield stress, M_{Ed} = design bending moment, $M_{f,Rd}$ = effective flange moment resistance, c = factor defined as:

$$c = a[0.17 + 3.5 \frac{b_f t_f}{2 f_{yf}} / \frac{t_w h_w}{2 f_{yw}}], \frac{c}{a} \leq 0.65$$

It is valid only if $M_{Ed} < M_{f,Rd}$. This formulation accounts for reduction of flange shear contribution due to bending and ensures safe design of thin-walled stainless steel members

4.2.1 PROPOSED EN1993-1-4 SHEAR DESIGN GUIDELINES BY DISSANAYAKE et

aL.– WITHOUT PERFORATION

Dissanayake[5] proposed a **web shear buckling reduction factor (χ_w)** for stainless steel lipped channel beams (LCBs) is shown in Figure 4.2. This was done to improve shear prediction by modifying based on FE and experimental results.

χ_w	
$\bar{\lambda}_w \leq 0.12$	2.1
$0.12 < \bar{\lambda}_w < 0.667$	$0.839/\bar{\lambda}_w^{0.433}$
$\bar{\lambda}_w \geq 0.667$	$1.797/(1.13 + \bar{\lambda}_w)$

4.2.2 PROPOSED EN1993-1-4 SHEAR DESIGN BY PERAMPALAM GATHEESHGAR et al.– WITH PERFORATION[21]

Gatheeshgar et al. (2023) [11]proposed an equivalent web thickness ($t_{w,eq}$) to enhance the shear strength prediction of cold-formed stainless steel (CFSS) lipped channel sections with circular web holes, aligning with Eurocode 3 (EN 1993-1-4) [40]design provisions.

$$t_{w,eq} = (1 - R^{1.43})^{0.72} \cdot t_w \quad (19)$$

$t_{w,eq}$ = equivalent web thickness, t_w = nominal web thickness, R = web hole ratio = $\frac{h_{\text{hole}}}{h_{\text{web}}}$.

5. RESULT AND DISCUSSION

The theoretical investigation shows that existing DSM, Eurocode 3, and Dissanayake–Gatheeshgar guidelines are unconservative for stainless steel lipped channel beams, especially when web openings exceed the AS/NZS 4600 limit of 150 mm. To overcome these shortcomings, modified shear design equations were developed, incorporating revised nominal shear strength, updated reduction factors, and an equivalent web thickness for perforated sections. These formulations, applicable to austenitic stainless steel with various perforation ratios, accurately capture the effects of perforation geometry and post-buckling behaviour. Overall, the proposed equations provide more reliable and conservative shear capacity predictions for cold-formed stainless steel members.

5.1 MODIFIED DSM AND EN1993-1-4 FOR PURE SHEAR

5.1.1 PROPOSED DSM DESIGN RULES FOR PURE SHEAR WITHOUT PERFORATION

$$\text{for } \lambda_v > 0.50: V_v = \left[1 - 0.13 \left(\frac{V_{cr}}{V_y} \right)^{0.4} \right] \left(\frac{V_{cr}}{V_y} \right)^{0.4} V_y \quad (20)$$

5.1.2 PROPOSED DSM DESIGN RULES FOR PURE SHEAR WITH PERFORATION

$v_{nl} = q_s \times v_v$, v_{nl} =nomial shear capacity(kN)

$$V_V = \left[1 - 0.15 \left(\frac{V_{cr}}{V_y} \right)^{0.4} \right] \left(\frac{V_{cr}}{V_y} \right)^{0.4} V_y \quad (21)$$

$V_y = 0.6 \times A_w \times f_y$

q_s is Shear Capacity Reduction factor = v_{nl}/v_v

$$q_s = 1 - 0.5 \left[\frac{d_{wh}}{d_1} \right] \text{ for } 0 < \frac{d_{wh}}{d_1} \leq 0.3 \quad (22)$$

$$q_s = 1.145 - 1.45 \left[\frac{d_{wh}}{d_1} \right] \text{ for } 0.4 < \frac{d_{wh}}{d_1} \leq 0.8 \quad (23)$$

5.1.3 PROPOSED EUROCODE 3 DESIGN RULES FOR PURE SHEAR WITHOUT PERFORATION

The sectional shear resistance, $V_{b,Rd}$, of a stainless steel member is calculated as the sum of the web shear resistance ($V_{bw,Rd}$) and flange shear resistance ($V_{bf,Rd}$)[40]:

$$V_{b,Rd} = V_{bw,Rd} + V_{bf,Rd} \leq \frac{\eta f_{yw} h_w t_w}{\sqrt{3} \gamma_{M1}} \quad (24)$$

$\eta = 1.2$ is a recommended factor for stainless steel , γ_{M1} = partial safety factor(1.1)

χ_w = web shear buckling reduction factor, which accounts for local buckling of the web.

	χ_w
$\lambda w \leq \frac{0.65}{\eta}$	η
$\frac{0.65}{\eta} < \lambda w < 0.65$	$\frac{0.65}{\lambda w}$
$\lambda w \geq 0.65$	$\leq \frac{1.92}{0.92 + \lambda w}$

The web slenderness, $\bar{\lambda}_w$, is defined for webs with transverse stiffeners at supports and mid-span as:

$$\bar{\lambda}_w = \frac{h_w}{t_w} \frac{1}{37.4 \epsilon \sqrt{k_\tau}} \quad (25)$$

with f_y = yield stress of stainless steel (or 0.2% proof stress), and E = modulus of elasticity (typically 210,000 N/mm²)., k_τ = web shear buckling coefficient for plates with rigid transverse stiffeners and without longitudinal stiffeners

$$k_\tau = 4.00 + 5.34 \left(\frac{a}{h_w} \right)^2 \text{ for } \frac{a}{h_w} < 1 \quad (26)$$

5.1.4 PROPOSED EUROCODE 3 DESIGN RULES FOR PURE SHEAR WITH PERFORATION

The **web shear resistance**, $V_{bw,Rd}$, is given by[40]:

$$V_{bw,Rd} = \frac{\chi_w f_{yw} h_w t_w}{\sqrt{3} \gamma_{M1}}$$

To enhance the EN1993-1-4 shear design accuracy for CFSS lipped channels with circular web holes, the web slenderness equation was modified by introducing an equivalent web thickness ($t_{w,eq}$). This equivalent thickness, defined as a function of the web hole ratio, replaces the actual web thickness (t_w) to account for the reduced effective area and ensure more reliable shear resistance predictions.

$$t_{w,eq} = (1 - R^{1.16})^{0.8} \cdot t_w \quad (27)$$

5.2 COMPARISON OF ULTIMATE SHEAR CAPACITY FROM FEM AND DSM AND EURO CODE WITHOUT PERFORATION

Table 4 Comparison of Ultimate Shear Capacity From FEM And DSM and Euro Code Without Perforation

S.N O	SECTON(mm)	Vu FEM	VnlWTA	VnlTTA	Vv Dissanayak	Vw Euro	Vnl DSM pro	Vw Euro Pro	VnlFEA /VWTA	VnlFEA/VnLTTA	VnlFEA/vn1 DSM Pro	Vv Dissanayake/VFE A	VFEA/VwPro
1	150x60x18x1.5	39.141	36.71	31.87	35.52	31.93	39.24	39.10	1.07	1.23	1.00	0.91	1.00
2	150x60x18x2	55.595	59.49	49.45	54.03	48.70	63.01	59.58	0.93	1.12	0.88	0.97	0.93
3	150x60x18x2.5	73.432	73.31	62.35	73.57	69.81	90.01	81.16	1.00	1.18	0.82	1.00	0.90
4	150x60x18x3	91.027	86.72	74.89	93.26	100.52	119.33	103.26	1.05	1.22	0.76	1.02	0.88
5	200x65x20x1.5	43.324	33.28	30.82	40.82	36.34	42.97	44.53	1.30	1.41	1.01	0.94	0.97
6	200x65x20x2	66.298	65.26	55.76	63.15	56.77	69.76	69.51	1.02	1.19	0.95	0.95	0.95
7	200x65x20x2.5	91.427	99.50	82.24	87.59	78.92	100.85	96.57	0.92	1.11	0.91	0.96	0.95
8	200x65x20x3	111.42	118.14	98.49	113.31	102.15	135.41	124.93	0.94	1.13	0.82	1.02	0.89
9	250x70x22x1.5	43.961	26.46	26.46	45.08	39.56	45.84	48.51	1.66	1.66	0.96	1.03	0.91
10	250x70x22x2	74.491	63.24	56.71	70.42	62.88	74.90	77.04	1.18	1.31	0.99	0.95	0.97
11	250x70x22x2.5	104.52	101.96	87.38	98.68	88.70	109.00	108.60	1.03	1.20	0.96	0.94	0.96
12	250x70x22x3	131.18	146.83	120.23	129.03	116.23	147.38	142.24	0.89	1.09	0.89	0.98	0.92
13	300x75x25x1.5	52.415	21.96	24.49	48.67	42.02	48.19	51.54	2.39	2.14	1.09	0.93	1.02
14	300x75x25x2	81.708	52.41	51.38	76.53	67.67	79.08	82.95	1.56	1.59	1.03	0.94	0.98
15	300x75x25x2.5	113.46	101.96	89.75	107.94	96.53	115.57	118.25	1.11	1.26	0.98	0.95	0.96
16	300x75x25x3	147.18	146.83	124.90	142.10	127.72	156.96	156.39	1.00	1.18	0.94	0.97	0.94
17	350x120x28x1.5	54.688	18.77	22.16	51.81	43.96	50.19	53.94	2.91	2.47	1.09	0.95	1.01
18	350x120x28x2	88.788	44.75	47.25	81.83	71.53	82.61	87.72	1.98	1.88	1.07	0.92	1.01
19	350x120x28x2.5	125.94	87.91	83.93	115.94	102.95	121.10	126.17	1.43	1.50	1.04	0.92	1.00
20	350x120x28x3	166.26	146.83	129.99	153.35	137.28	164.97	168.16	1.13	1.28	1.01	0.92	0.99

5.3 COMPARISON OF ULTIMATE SHEAR CAPACITY FROM FEM AND DSM AND EURO CODE WITH PERFORATION

Table 5 Comparison of Ultimate Shear Capacity With Perforation

S.N O	SECTON	Dwh	Vfea	Vnl With tension field	Vnl Without tension field	Vnl Euro	Vnl DSM Pro	VEuro Pro	VFEA/VW TF	VFEA/V WTTF	VFEA/V euro	VFEA/ VDSM (Pro)	VFEA/VE uro(Pro)
1	150x60x18x1.5	0.2	33.91	28.02	33.74	28.41	30.73	33.15	1.21	1.00	0.84	0.91	0.98
2	150x60x18x1.5	0.4	24.41	23.40	26.40	22.45	22.11	25.17	1.04	1.08	0.92	0.91	1.03
3	150x60x18x1.5	0.6	16.23	18.79	16.31	15.07	14.34	16.39	0.86	1.00	0.93	0.88	1.01
4	150x60x18x1.5	0.8	9.91	14.18	6.22	6.90	8.44	7.00	0.70	0.63	0.70	0.85	0.71
5	150x60x18x2	0.2	51.22	33.58	53.76	43.57	52.53	51.88	1.53	1.05	0.85	1.03	1.01
6	150x60x18x2	0.4	37.65	28.05	42.07	34.82	37.88	39.77	1.34	1.12	0.92	1.01	1.06
7	150x60x18x2	0.6	25.36	22.52	25.99	23.80	24.61	25.91	1.13	1.02	0.94	0.97	1.02
8	150x60x18x2	0.8	14.04	17.00	9.91	11.24	12.02	11.41	0.83	0.71	0.80	0.86	0.81
9	150x60x18x2.5	0.2	67.10	32.64	76.18	59.66	65.98	71.08	2.06	1.14	0.89	0.98	1.06
10	150x60x18x2.5	0.4	52.08	27.27	59.61	48.10	50.37	54.98	1.91	1.14	0.92	0.97	1.06
11	150x60x18x2.5	0.6	34.31	21.89	36.82	33.36	33.58	36.34	1.57	1.07	0.97	0.98	1.06
12	150x60x18x2.5	0.8	20.27	16.52	14.04	16.18	16.79	16.43	1.23	0.69	0.80	0.83	0.81
13	150x60x18x3	0.2	83.47	31.71	100.09	76.21	78.05	90.85	2.63	1.20	0.91	0.94	1.09
14	150x60x18x3	0.4	66.57	26.49	78.32	61.88	59.58	70.77	2.51	1.18	0.93	0.89	1.06
15	150x60x18x3	0.6	45.28	21.27	48.39	43.44	39.72	47.34	2.13	1.07	0.96	0.88	1.05
16	150x60x18x3	0.8	25.78	16.05	18.45	21.54	19.86	21.89	1.61	0.72	0.84	0.77	0.85
17	200x65x20x1.5	0.2	40.37	33.28	37.15	32.15	48.93	38.22	1.21	0.92	0.80	1.21	0.95
18	200x65x20x1.5	0.4	28.17	28.59	29.07	25.13	35.24	28.66	0.99	1.03	0.89	1.25	1.02
19	200x65x20x1.5	0.6	18.06	22.95	17.96	16.59	22.86	18.03	0.79	0.99	0.92	1.27	1.00
20	200x65x20x1.5	0.8	9.30	17.32	6.85	7.39	11.16	7.50	0.54	0.74	0.79	1.20	0.81

S.N O	SECTON	Dwh	Vfea	Vnl With tension field	Vnl Without tension field	Vnl Euro	Vnl DSM Pro	VEuro Pro	VFEA/VW TF	VFEA/V WTTF	VFEA/V euro	VFEA/VDSM (Pro)	VFEA/VE uro(Pro)
21	200x65x20x2	0.2	60.27	49.81	59.98	50.50	67.66	60.08	1.21	1.00	0.84	1.12	1.00
22	200x65x20x2	0.4	44.81	41.61	46.94	39.90	48.77	45.54	1.08	1.05	0.89	1.09	1.02
23	200x65x20x2	0.6	28.36	33.41	29.00	26.79	31.64	29.13	0.85	1.02	0.94	1.12	1.03
24	200x65x20x2	0.8	15.32	25.21	11.06	12.27	15.46	12.44	0.61	0.72	0.80	1.01	0.81
25	200x65x20x2.5	0.2	80.55	60.12	86.22	70.53	86.77	83.96	1.34	1.07	0.88	1.08	1.04
26	200x65x20x2.5	0.4	60.10	50.22	67.47	56.21	62.58	64.20	1.20	1.12	0.94	1.04	1.07
27	200x65x20x2.5	0.6	40.16	40.33	41.68	38.27	40.62	41.64	1.00	1.04	0.95	1.01	1.04
28	200x65x20x2.5	0.8	21.95	30.43	15.89	17.94	19.84	18.21	0.72	0.72	0.82	0.90	0.83
29	200x65x20x3	0.2	101.67	58.86	115.07	91.62	106.32	109.13	1.73	1.13	0.90	1.05	1.07
30	200x65x20x3	0.4	77.72	49.17	90.05	73.55	81.16	84.05	1.58	1.16	0.95	1.04	1.08
31	200x65x20x3	0.6	52.21	39.48	55.63	50.66	54.11	55.17	1.32	1.07	0.97	1.04	1.06
32	200x65x20x3	0.8	28.50	29.79	21.21	24.26	27.05	24.63	0.96	0.74	0.85	0.95	0.86
33	250x70x22x1.5	0.2	40.73	26.46	39.76	34.86	59.32	41.42	1.54	0.98	0.86	1.46	1.02
34	250x70x22x1.5	0.4	31.91	26.46	31.11	27.04	42.71	30.82	1.21	0.98	0.85	1.34	0.97
35	250x70x22x1.5	0.6	19.93	22.95	19.22	17.65	27.69	19.17	0.87	0.96	0.89	1.39	0.96
36	250x70x22x1.5	0.8	9.74	17.32	7.33	7.72	13.51	7.82	0.56	0.75	0.79	1.39	0.80
37	250x70x22x2	0.2	68.62	60.84	64.69	55.70	82.20	66.23	1.13	0.94	0.81	1.20	0.97
38	250x70x22x2	0.4	48.07	50.82	50.62	43.64	59.19	49.78	0.95	1.05	0.91	1.23	1.04
39	250x70x22x2	0.6	30.59	40.81	31.27	28.92	38.40	31.43	0.75	1.02	0.95	1.26	1.03
40	250x70x22x2	0.8	16.19	30.79	11.92	12.96	18.74	13.14	0.53	0.74	0.80	1.16	0.81

S.N O	SECTON	Dwh	Vfea	Vnl With tension field	Vnl Without tension field	Vnl Euro	Vnl DSM Pro	VEuro Pro	VFEA/VW TF	VFEA/V WTTF	VFEA/V euro	VFEA/VDSM (Pro)	VFEA/VE uro(Pro)
41	250x70x22x2.5	0.2	91.79	77.82	93.73	78.91	105.65	93.88	1.18	1.02	0.86	1.15	1.02
42	250x70x22x2.5	0.4	67.88	65.01	73.34	62.35	76.11	71.16	1.04	1.08	0.92	1.12	1.05
43	250x70x22x2.5	0.6	44.08	52.20	45.31	41.85	49.37	45.52	0.84	1.03	0.95	1.12	1.03
44	250x70x22x2.5	0.8	23.60	39.39	17.28	19.17	24.11	19.44	0.60	0.73	0.81	1.02	0.82
45	250x70x22x3	0.2	120.08	92.61	126.15	103.79	129.49	123.54	1.30	1.05	0.86	1.08	1.03
46	250x70x22x3	0.4	87.70	77.37	98.71	82.58	93.30	94.31	1.13	1.13	0.94	1.06	1.08
47	250x70x22x3	0.6	58.05	62.12	60.98	56.07	60.54	61.01	0.93	1.05	0.97	1.04	1.05
48	250x70x22x3	0.8	30.67	46.88	23.25	26.18	29.56	26.57	0.65	0.76	0.85	0.96	0.87
49	300x75x25x1.5	0.2	47.57	21.96	41.89	36.92	69.35	43.84	2.17	0.88	0.78	1.46	0.92
50	300x75x25x1.5	0.4	34.98	21.96	32.78	28.47	49.90	32.44	1.59	0.94	0.81	1.43	0.93
51	300x75x25x1.5	0.6	21.56	21.96	20.25	18.42	32.35	20.00	0.98	0.94	0.85	1.50	0.93
52	300x75x25x1.5	0.8	10.29	17.32	7.72	7.95	15.39	8.05	0.59	0.75	0.77	1.50	0.78
53	300x75x25x2	0.2	72.83	52.41	68.50	59.75	96.23	71.00	1.39	0.94	0.82	1.32	0.97
54	300x75x25x2	0.4	53.42	50.82	53.60	46.51	69.27	53.03	1.05	1.00	0.87	1.30	0.99
55	300x75x25x2	0.6	33.28	40.81	33.11	30.51	44.91	33.15	0.82	0.99	0.92	1.35	1.00
56	300x75x25x2	0.8	16.67	30.79	12.63	13.46	21.38	13.64	0.54	0.76	0.81	1.28	0.82
57	300x75x25x2.5	0.2	100.38	94.04	99.74	85.58	123.87	101.76	1.07	0.99	0.85	1.23	1.01
58	300x75x25x2.5	0.4	76.96	78.56	78.05	67.15	89.18	76.61	0.98	1.01	0.87	1.16	1.00
59	300x75x25x2.5	0.6	46.58	63.08	48.22	44.59	57.83	48.48	0.74	1.04	0.96	1.24	1.04
60	300x75x25x2.5	0.8	24.91	47.60	18.38	20.06	28.23	20.34	0.52	0.74	0.81	1.13	0.82

S.N O	SECTON	Dwh	Vfea	Vnl With tension field	Vnl Without tension field	Vnl Euro	Vnl DSM Pro	VEuro Pro	VFEA/VW TF	VFEA/V WTTF	VFEA/V euro	VFEA/ VDSM (Pro)	VFEA/VE uro(Pro)
61	300x75x25x3	0.2	124.66	112.07	134.97	113.63	152.06	135.19	1.11	1.08	0.91	1.22	1.08
62	300x75x25x3	0.4	99.65	93.62	105.61	89.78	109.49	102.47	1.06	1.06	0.90	1.10	1.03
63	300x75x25x3	0.6	62.90	75.17	65.24	60.27	71.02	65.55	0.84	1.04	0.96	1.13	1.04
64	300x75x25x3	0.8	33.55	56.72	24.88	27.60	34.67	28.00	0.59	0.74	0.82	1.03	0.83
65	350x120x28x1.5	0.2	50.73	18.77	43.70	38.53	79.21	45.74	2.70	0.86	0.76	1.56	0.90
66	350x120x28x1.5	0.4	37.47	18.77	34.20	29.58	57.06	33.69	2.00	0.91	0.79	1.52	0.90
67	350x120x28x1.5	0.6	23.78	18.77	21.13	19.01	37.00	20.63	1.27	0.89	0.80	1.56	0.87
68	350x120x28x1.5	0.8	11.20	17.32	8.06	8.12	18.03	8.23	0.65	0.72	0.73	1.61	0.73
69	350x120x28x2	0.2	80.07	44.75	71.70	62.98	110.04	74.82	1.79	0.90	0.79	1.37	0.93
70	350x120x28x2	0.4	58.07	44.75	56.11	48.78	79.29	55.59	1.30	0.97	0.84	1.37	0.96
71	350x120x28x2	0.6	36.08	40.81	34.66	31.75	51.40	34.49	0.88	0.96	0.88	1.42	0.96
72	350x120x28x2	0.8	17.60	30.79	13.22	13.84	25.05	14.02	0.57	0.75	0.79	1.42	0.80
73	350x120x28x2.5	0.2	111.83	87.91	104.78	91.00	141.79	108.17	1.27	0.94	0.81	1.27	0.97
74	350x120x28x2.5	0.4	85.59	79.41	81.99	71.01	102.19	80.98	1.08	0.96	0.83	1.19	0.95
75	350x120x28x2.5	0.6	53.53	63.76	50.65	46.76	66.26	50.81	0.84	0.95	0.87	1.24	0.95
76	350x120x28x2.5	0.8	25.82	48.11	19.31	20.75	32.31	21.03	0.54	0.75	0.80	1.25	0.81
77	350x120x28x3	0.2	145.32	131.52	142.30	121.77	174.22	144.81	1.10	0.98	0.84	1.20	1.00
78	350x120x28x3	0.4	105.36	109.87	111.35	95.65	125.58	109.13	0.96	1.06	0.91	1.19	1.04
79	350x120x28x3	0.6	70.65	88.22	68.79	63.63	81.44	69.17	0.80	0.97	0.90	1.15	0.98
80	350x120x28x3	0.8	35.75	66.57	26.23	73.05	39.72	29.10	0.54	0.73	2.04	1.11	0.81

5.4 COMPARISON OF SHEAR CAPACITY REDUCTION FACTOR FROM FEM AND DSM AND EURO CODE

Table 6 Comparison of Shear Capacity Reduction Factor

S.N O	SECTON	Dwh	qsfea	qs With tension field	qs Without tension field	teq Euro Pro	qs DSM Pro	teq Euro Disaanky pro	qsFEA/qsW TF	qsFEA/qsTTF	qsFEA/qs Pro)
1	150x60x18x1.5	0.2	0.88	0.76	0.88	1.31	0.90	1.31	1.16	1.00	0.98
2	150x60x18x1.5	0.4	0.64	0.64	0.69	1.08	0.69	1.08	1.00	0.92	0.93
3	150x60x18x1.5	0.6	0.42	0.51	0.43	0.82	0.46	0.82	0.83	1.00	0.92
4	150x60x18x1.5	0.8	0.26	0.39	0.16	0.48	0.23	0.48	0.67	1.59	1.13
5	150x60x18x2	0.2	0.84	0.56	0.88	1.78	0.90	1.78	1.49	0.95	0.93
6	150x60x18x2	0.4	0.62	0.47	0.69	1.47	0.69	1.47	1.31	0.89	0.90
7	150x60x18x2	0.6	0.42	0.38	0.43	1.10	0.46	1.10	1.10	0.98	0.91
8	150x60x18x2	0.8	0.23	0.29	0.16	0.65	0.23	0.65	0.80	1.42	1.00
9	150x60x18x2.5	0.2	0.78	0.45	0.88	2.23	0.90	2.23	1.74	0.88	0.86
10	150x60x18x2.5	0.4	0.60	0.37	0.69	1.84	0.69	1.84	1.62	0.87	0.88
11	150x60x18x2.5	0.6	0.40	0.30	0.43	1.37	0.46	1.37	1.33	0.93	0.87
12	150x60x18x2.5	0.8	0.23	0.23	0.16	0.81	0.23	0.81	1.04	1.44	1.02
13	150x60x18x3	0.2	0.73	0.37	0.88	2.67	0.90	2.67	2.01	0.83	0.82
14	150x60x18x3	0.4	0.59	0.31	0.69	2.21	0.69	2.21	1.92	0.85	0.85
15	150x60x18x3	0.6	0.40	0.25	0.43	1.65	0.46	1.65	1.62	0.94	0.87
16	150x60x18x3	0.8	0.23	0.19	0.16	0.97	0.23	0.97	1.22	1.40	0.99
17	200x65x20x1.5	0.2	0.96	1	0.88	1.34	0.90	1.34	0.96	1.09	1.06
18	200x65x20x1.5	0.4	0.67	0.86	0.69	1.10	0.69	1.10	0.78	0.97	0.97
19	200x65x20x1.5	0.6	0.43	0.69	0.43	0.82	0.46	0.82	0.62	1.01	0.93
20	200x65x20x1.5	0.8	0.22	0.52	0.16	0.48	0.23	0.48	0.42	1.36	0.96

S.N O	SECTON	Dwh	qsfea	qs With tension field	qs Without tension field	teq Euro Pro	qs DSM Pro	teq Euro Disaanky pro	qsFEA/qsW TF	qsFEA/qsTTF	qsFEA/qs Pro)
21	200x65x20x2	0.2	0.88	0.76	0.88	1.78	0.90	1.78	1.16	1.00	0.98
22	200x65x20x2	0.4	0.66	0.64	0.69	1.47	0.69	1.47	1.03	0.95	0.96
23	200x65x20x2	0.6	0.42	0.51	0.43	1.10	0.46	1.10	0.81	0.98	0.91
24	200x65x20x2	0.8	0.22	0.39	0.16	0.65	0.23	0.65	0.58	1.39	0.98
25	200x65x20x2.5	0.2	0.82	0.60	0.88	2.23	0.90	2.23	1.36	0.93	0.91
26	200x65x20x2.5	0.4	0.61	0.50	0.69	1.84	0.69	1.84	1.22	0.89	0.89
27	200x65x20x2.5	0.6	0.41	0.41	0.43	1.37	0.46	1.37	1.01	0.96	0.89
28	200x65x20x2.5	0.8	0.22	0.31	0.16	0.81	0.23	0.81	0.73	1.38	0.98
29	200x65x20x3	0.2	0.78	0.50	0.88	2.67	0.90	2.67	1.56	0.88	0.86
30	200x65x20x3	0.4	0.59	0.42	0.69	2.21	0.69	2.21	1.43	0.86	0.87
31	200x65x20x3	0.6	0.40	0.33	0.43	1.65	0.46	1.65	1.19	0.94	0.87
32	200x65x20x3	0.8	0.22	0.25	0.16	0.97	0.23	0.97	0.86	1.34	0.95
33	250x70x22x1.5	0.2	0.90	1	0.88	1.34	0.90	1.34	0.90	1.02	1.00
34	250x70x22x1.5	0.4	0.71	1	0.69	1.10	0.69	1.10	0.71	1.03	1.03
35	250x70x22x1.5	0.6	0.44	0.87	0.43	0.82	0.46	0.82	0.51	1.04	0.96
36	250x70x22x1.5	0.8	0.22	0.65	0.16	0.48	0.23	0.48	0.33	1.33	0.94
37	250x70x22x2	0.2	0.93	0.96	0.88	1.78	0.90	1.78	0.97	1.06	1.04
38	250x70x22x2	0.4	0.65	0.80	0.69	1.47	0.69	1.47	0.81	0.95	0.95
39	250x70x22x2	0.6	0.42	0.65	0.43	1.10	0.46	1.10	0.64	0.98	0.91
40	250x70x22x2	0.8	0.22	0.49	0.16	0.65	0.23	0.65	0.45	1.36	0.96

S.N O	SECTON	Dwh	qsfea	qs With tension field	qs Without tension field	teq Euro Pro	qs DSM Pro	teq Euro Disaanky pro	qsFEA/qsW TF	qsFEA/qsTTF	qsFEA/qs Pro)
41	250x70x22x2.5	0.2	0.86	0.76	0.88	2.23	0.90	2.23	1.13	0.98	0.96
42	250x70x22x2.5	0.4	0.64	0.64	0.69	1.84	0.69	1.84	1.00	0.93	0.93
43	250x70x22x2.5	0.6	0.41	0.51	0.43	1.37	0.46	1.37	0.81	0.97	0.90
44	250x70x22x2.5	0.8	0.22	0.39	0.16	0.81	0.23	0.81	0.57	1.37	0.97
45	250x70x22x3	0.2	0.84	0.63	0.88	2.67	0.90	2.67	1.33	0.95	0.93
46	250x70x22x3	0.4	0.61	0.53	0.69	2.21	0.69	2.21	1.16	0.89	0.89
47	250x70x22x3	0.6	0.40	0.42	0.43	1.65	0.46	1.65	0.96	0.95	0.88
48	250x70x22x3	0.8	0.21	0.32	0.16	0.97	0.23	0.97	0.67	1.32	0.93
49	300x75x25x1.5	0.2	1.00	1	0.88	1.34	0.90	1.34	1.00	1.14	1.11
50	300x75x25x1.5	0.4	0.73	1	0.69	1.10	0.69	1.10	0.73	1.07	1.07
51	300x75x25x1.5	0.6	0.45	1	0.43	0.82	0.46	0.82	0.45	1.06	0.99
52	300x75x25x1.5	0.8	0.22	0.79	0.16	0.48	0.23	0.48	0.27	1.33	0.94
53	300x75x25x2	0.2	0.94	1	0.88	1.78	0.90	1.78	0.94	1.06	1.04
54	300x75x25x2	0.4	0.69	0.97	0.69	1.47	0.69	1.47	0.71	1.00	1.00
55	300x75x25x2	0.6	0.43	0.78	0.43	1.10	0.46	1.10	0.55	1.01	0.93
56	300x75x25x2	0.8	0.21	0.59	0.16	0.65	0.23	0.65	0.36	1.32	0.94
57	300x75x25x2.5	0.2	0.89	0.92	0.88	2.23	0.90	2.23	0.96	1.01	0.98
58	300x75x25x2.5	0.4	0.68	0.77	0.69	1.84	0.69	1.84	0.88	0.99	0.99
59	300x75x25x2.5	0.6	0.41	0.62	0.43	1.37	0.46	1.37	0.66	0.97	0.90
60	300x75x25x2.5	0.8	0.22	0.47	0.16	0.81	0.23	0.81	0.47	1.35	0.96

S.N O	SECTON	Dwh	qsfea	qs With tension field	qs Without tension field	teq Euro Pro	qs DSM Pro	teq Euro Disaanky pro	qsFEA/qsW TF	qsFEA/qsTTF	qsFEA/qs Pro)
61	300x75x25x3	0.2	0.81	0.76	0.88	2.67	0.90	2.67	1.06	0.92	0.90
62	300x75x25x3	0.4	0.65	0.64	0.69	2.21	0.69	2.21	1.02	0.94	0.95
63	300x75x25x3	0.6	0.41	0.51	0.43	1.65	0.46	1.65	0.80	0.96	0.90
64	300x75x25x3	0.8	0.22	0.39	0.16	0.97	0.23	0.97	0.57	1.35	0.96
65	350x120x28x1.5	0.2	1.02	1	0.88	1.34	0.90	1.34	1.02	1.16	1.13
66	350x120x28x1.5	0.4	0.75	1	0.69	1.10	0.69	1.10	0.75	1.10	1.10
67	350x120x28x1.5	0.6	0.48	1	0.43	0.82	0.46	0.82	0.48	1.13	1.05
68	350x120x28x1.5	0.8	0.23	0.92	0.16	0.48	0.23	0.48	0.24	1.39	0.98
69	350x120x28x2	0.2	0.98	1	0.88	1.78	0.90	1.78	0.98	1.12	1.09
70	350x120x28x2	0.4	0.71	1	0.69	1.47	0.69	1.47	0.71	1.03	1.04
71	350x120x28x2	0.6	0.44	0.91	0.43	1.10	0.46	1.10	0.49	1.04	0.97
72	350x120x28x2	0.8	0.22	0.69	0.16	0.65	0.23	0.65	0.31	1.33	0.94
73	350x120x28x2.5	0.2	0.94	1	0.88	2.23	0.90	2.23	0.94	1.07	1.04
74	350x120x28x2.5	0.4	0.72	0.90	0.69	1.84	0.69	1.84	0.80	1.04	1.05
75	350x120x28x2.5	0.6	0.45	0.73	0.43	1.37	0.46	1.37	0.62	1.06	0.98
76	350x120x28x2.5	0.8	0.22	0.55	0.16	0.81	0.23	0.81	0.40	1.34	0.95
77	350x120x28x3	0.2	0.90	0.90	0.88	2.67	0.90	2.67	1.00	1.02	1.00
78	350x120x28x3	0.4	0.65	0.75	0.69	2.21	0.69	2.21	0.87	0.95	0.95
79	350x120x28x3	0.6	0.44	0.60	0.43	1.65	1.65	0.73	1.03	0.27	0.27
80	350x120x28x3	0.8	0.22	0.45	0.16	0.97	0.97	0.49	1.36	0.23	0.23

COMPARISON OF ULTIMATE SHEAR CAPACITY FROM FEM AND DSM AND EURO CODE WITHOUT PERFORATION

Table 4 shows that FE shear capacities for unperforated lipped channel beams align closely with analytical predictions when tension field action is included, highlighting the importance of post-buckling behaviour. Thin sections exhibit higher FE capacities than predictions without TFA, reflecting the conservatism of conventional methods. The proposed DSM and modified Eurocode equations provide the most accurate results, with FE-to-predicted ratios near unity due to improved web slenderness and effective thickness modelling. For thicker sections, numerical and analytical values converge, demonstrating consistent accuracy across all thicknesses. Overall, the proposed formulations outperform existing codes by realistically capturing shear buckling and post-buckling mechanisms.

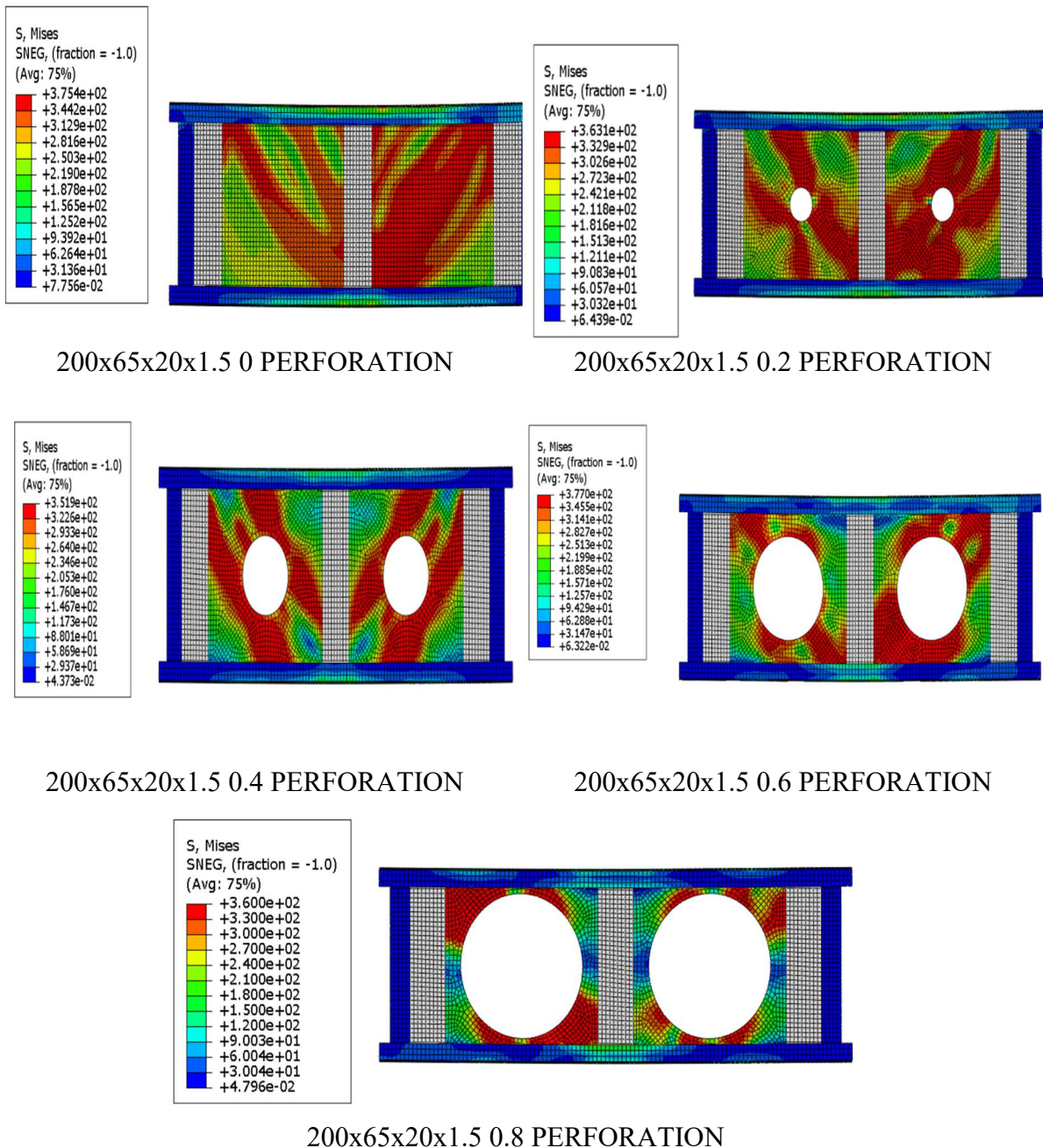
DISCUSSION ON COMPARISON OF SHEAR CAPACITY FROM FEM AND DSM AND EURO CODE

Table 5 demonstrates that shear capacity decreases progressively with increasing perforation ratio, with moderate reductions for small openings ($dwh \leq 0.4$) and severe losses for larger openings ($dwh \geq 0.6$) due to reduced stiffness and effective shear area. Analytical models without tension field action consistently underpredict FE results, especially for smaller perforations where diagonal tension still develops. The proposed DSM and modified Eurocode equations show the closest agreement with FE capacities across all perforation levels, owing to improved modelling of perforation-dependent slenderness and shear buckling behaviour. The nonlinear capacity reduction beyond $dwh = 0.5$ further highlights the necessity for modified design factors for beams with significant web openings.

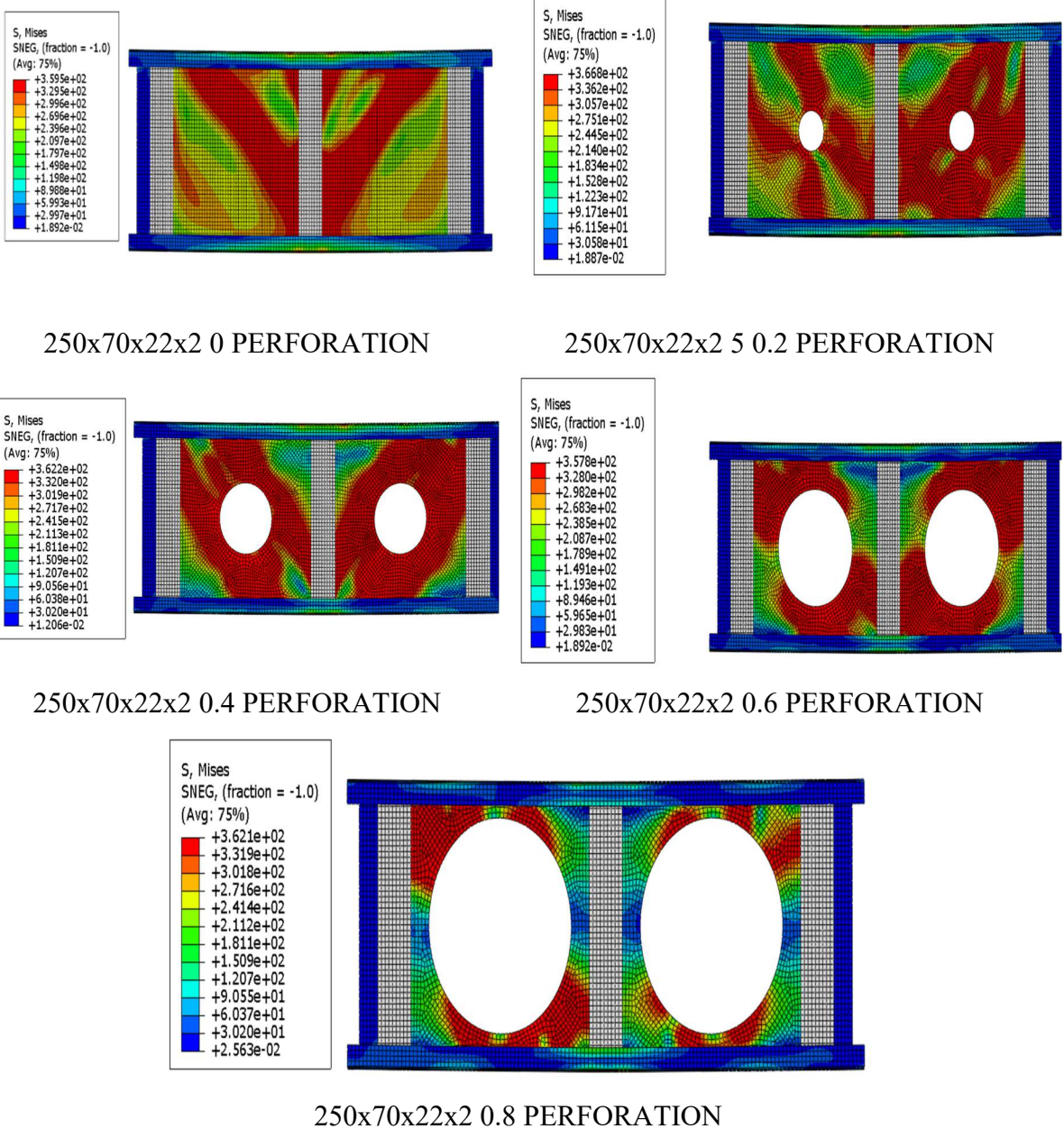
COMPARISON OF SHEAR CAPACITY REDUCTION FACTOR FROM FEM AND DSM AND EURO CODE

Table 6 shows that the shear capacity reduction factor (qs) decreases sharply with increasing perforation ratio, with minimal loss for small openings ($dwh = 0.2$) but a severe reduction to nearly 25–30% of the original capacity at $dwh = 0.8$. This nonlinear trend highlights the significant weakening of the web as the perforation disrupts the shear flow path. Conventional analytical methods underestimate qs , especially at higher perforation levels, due to their inability to capture stress redistribution around openings. In contrast, the proposed DSM and modified Eurocode equations, using an equivalent web slenderness approach, closely match FE results with qs ratios near unity.

5.5 NON-LINEAR FE ANALYSIS SHEAR FAILURE



**Figure 6(a) Non-linear FE analysis shear failure for section LCB
200x65x20x1.5mm**



**Figure 6 (b) Non-linear FE analysis shear failure for section LCB
250x70x22x2mm**

The nonlinear FE analysis reveals that web perforations have a substantial influence on the shear failure behaviour of cold-formed stainless steel LCBs. The unperforated sections exhibited a distinct diagonal tension band characteristic of classical shear buckling with effective post-buckling resistance. As the perforation ratio increased, the stress flow became progressively disturbed, with pronounced stress concentrations forming around the hole boundaries. Smaller openings (ratios 0.2 and 0.4) were still able to sustain partial tension field action, whereas larger openings (0.6 and 0.8) disrupted the continuity of the tension band,

resulting in localized yielding, web distortion, and an early decline in stiffness as depicted in Figure 6 . Across all section sizes analysed, failure consistently followed the diagonal tension path, although its intensity weakened as the perforation size increased. Overall, the results confirm that larger perforations significantly reduce shear capacity by diminishing the effective web area and interrupting the principal tension-transfer mechanism.

5.6 SHEAR CAPACITY VS PERFORATION RATIO

Figures 7 (a) and (b) illustrate the relationship between shear capacity and perforation ratio for different lipped channel beam (LCB) sections. The FEA results plotted for perforation ratios ranging from 0.2 to 0.8 indicate that the shear capacity decreases steadily with an increase in perforation ratio. This reduction occurs because larger web openings diminish the effective shear area of the beam. Beams with greater web depth and thickness show higher shear capacities due to their stronger load-carrying ability. The results also confirm that shear capacity and perforation ratio are inversely proportional, while shear capacity increases with web depth.

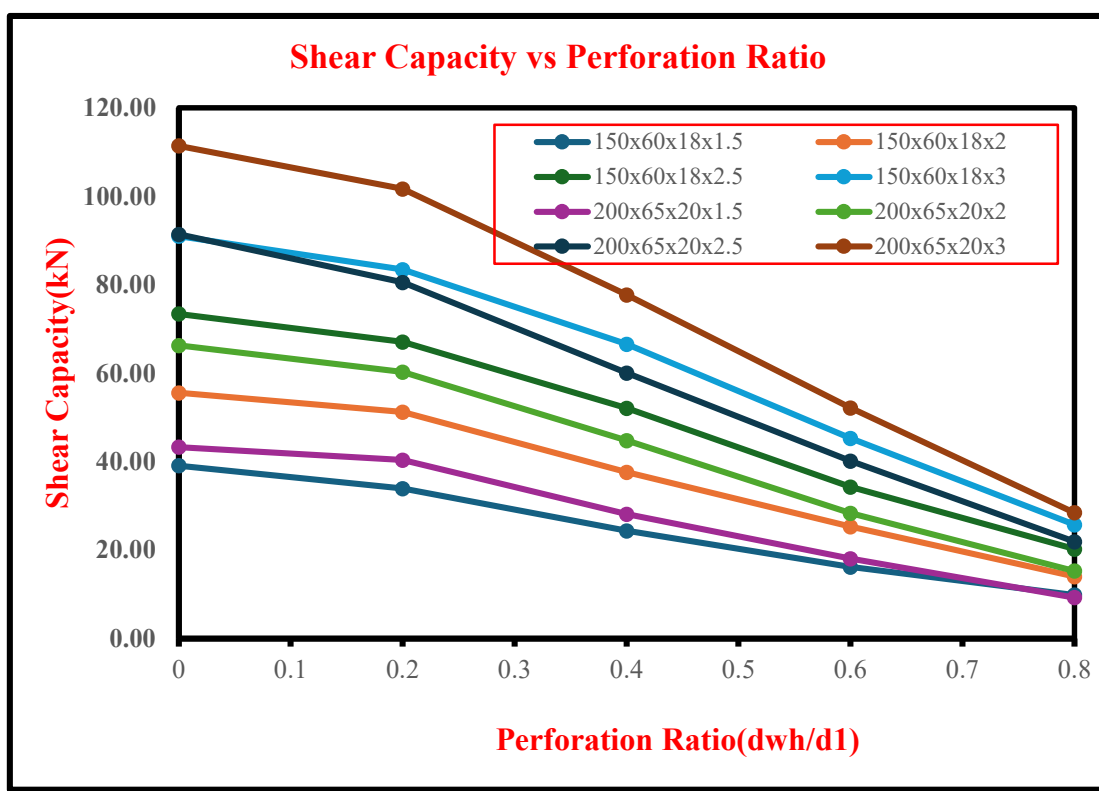


Figure 7 (a) Shear Capacity vs Perforation Plot from FEA

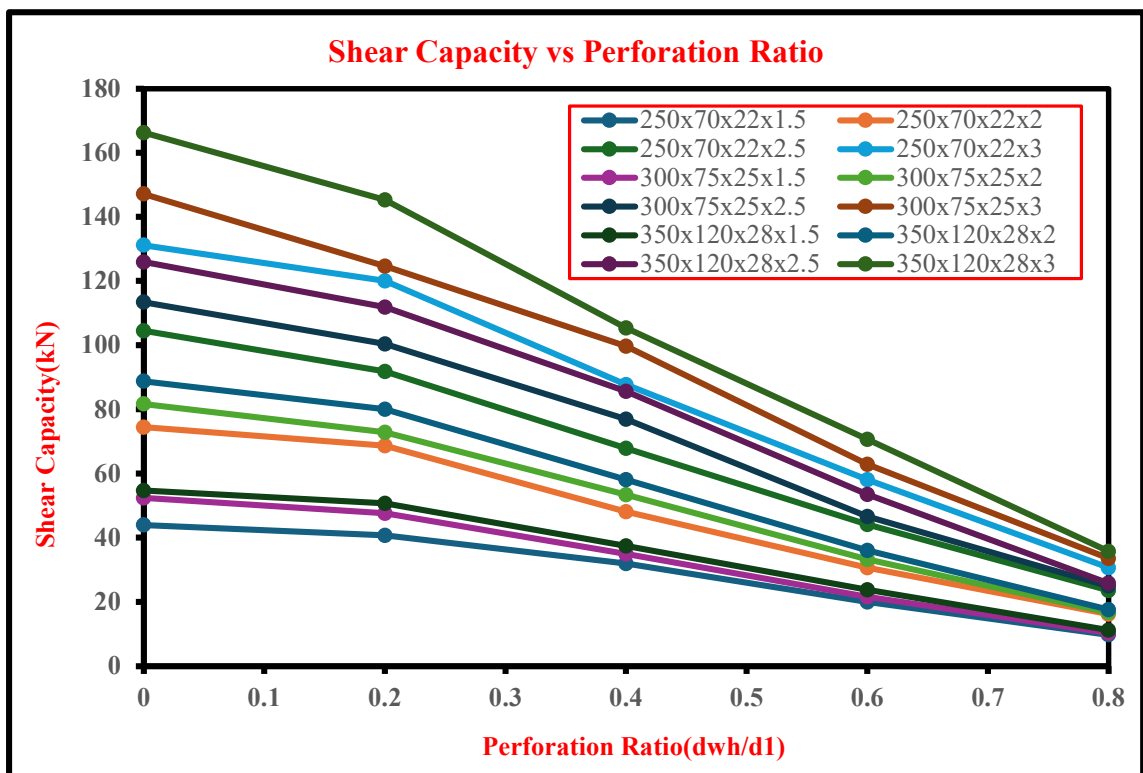


Figure 7 (b) Shear Capacity vs Perforation Plot from FEA

5.7 SHEAR CAPACITY VS DISPLACEMENT

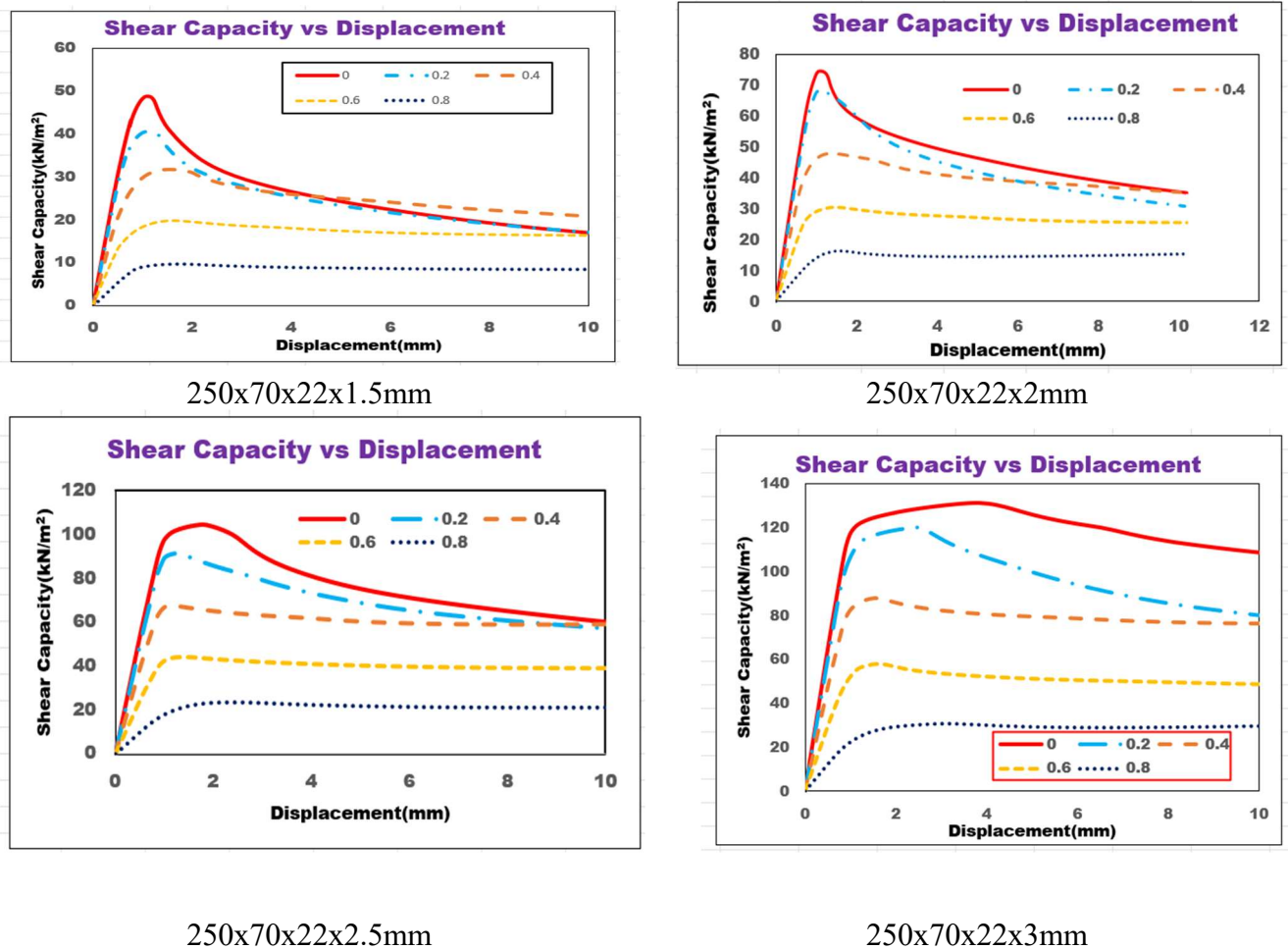


Figure 8 Shear Capacity vs Displacement Plot

Figure 8 presents the variation of shear capacity with displacement for cold-formed Stainless Steel lipped channel beams (SSLCBs) of dimensions $250 \times 70 \times 22$ with different thicknesses of 1.5 mm, 2 mm, 2.5 mm, and 3 mm. Each plot shows the shear response for different perforation ratios ranging from 0 (solid web) to 0.8. It is evident that the shear capacity increases significantly with an increase in section thickness, indicating that thicker webs possess higher stiffness and resistance against shear buckling. The beam with a thickness of 1.5 mm shows a maximum shear capacity of around 50 kN/mm^2 , while the 3 mm section attains more than 130 kN/m^2 . However, as the perforation ratio increases, a noticeable reduction in shear capacity occurs for all thicknesses due to the reduction of the effective web area and the introduction of stress concentration around the openings, which initiate earlier local buckling. The curves display an initial linear rise up to the peak load followed by a gradual decline, representing the

post-buckling strength governed by tension field action. Sections with smaller perforations maintain higher residual strength, while those with larger openings show a steeper capacity drop. Additionally, the displacement corresponding to the peak load increases with section thickness, reflecting improved ductility. Overall, the results clearly demonstrate that both web thickness and perforation ratio have a pronounced effect on the shear performance of LCBs, with thicker sections and smaller openings providing superior shear strength and deformation capacity.

5.8 SHEAR CAPACITY COMPARISON PLOT FOR FEM AND DSM AND EURO CODE WITHOUT PERFORATION

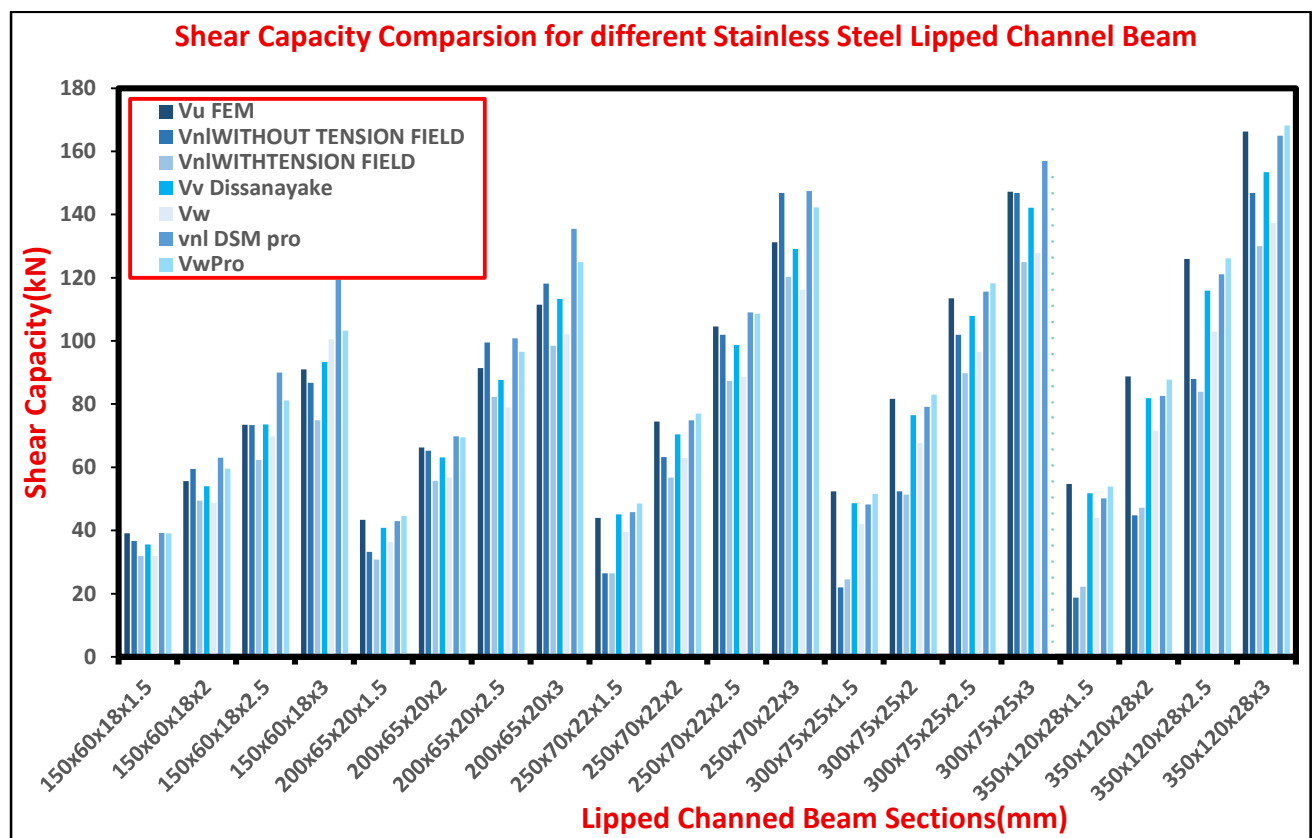


Figure 9 Shear Capacity Comparison for different Stainless Steel Lipped Channel Beam

Figure 9 illustrates a comparative analysis of the shear capacity of different cold-formed stainless steel lipped channel beams obtained from various prediction methods and finite element (FE) results. The comparison includes shear strengths derived from finite element analysis (Vu FEM), nominal shear strength without and with tension field action (Vnl Without Tension Field and Vnl With Tension Field), Dissanayake's design model (Vv Dissanayake), web shear strength (Vw), DSM proposed equation (Vnl DSM_{pro}), and proposed web shear strength (Vw_{Pro}). The beam sections analyzed range from 150×60×18×1.5 mm to

$350 \times 120 \times 28 \times 3$ mm, covering a wide range of section geometries and thicknesses. The nominal strengths without tension field action show significantly lower values, highlighting the conservative nature of design when post-buckling strength is neglected. When tension field action is incorporated, the predicted shear capacities increase and align more closely with FEM results, demonstrating the importance of accounting for post-buckling strength in stainless steel members.

5.9 SHEAR CAPACITY COMPARISON PLOT FOR FEM AND DSM AND EURO CODE WITH PERFORATION

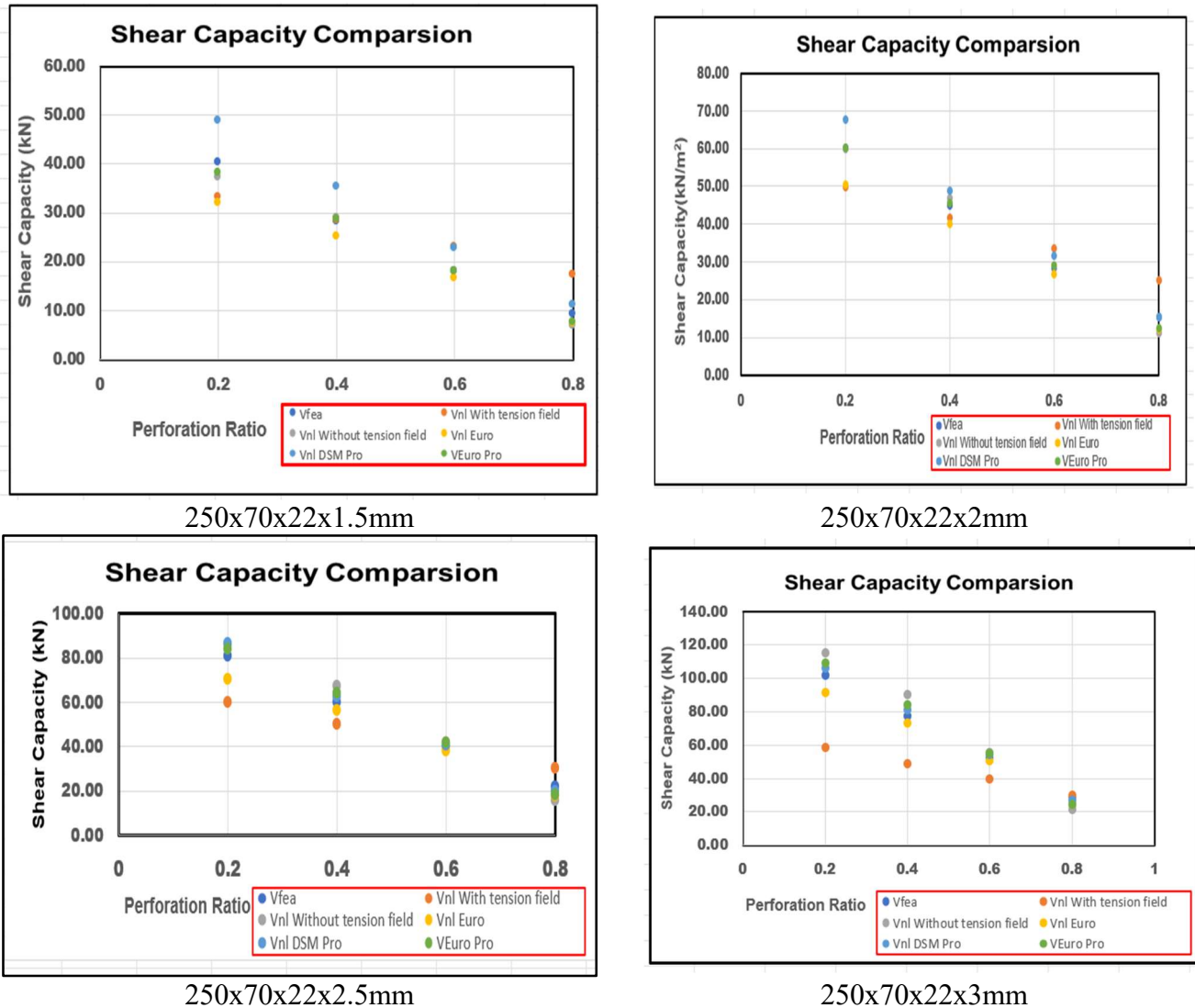


Figure 10 Shear Capacity Comparison for different Stainless Steel Lipped Channel Beam with Perforation

Figure 10 compares the shear capacities of cold-formed stainless steel lipped channel beams with different thicknesses (1.5–3 mm) and perforation ratios (0–0.8) using FEM, DSM,

and Eurocode predictions. Results show that shear capacity decreases with increasing perforation ratio due to the reduction in effective web area. Among the methods, the FEM results show the highest and most realistic values as they capture post-buckling and tension field effects accurately. The DSM predictions show better agreement with FEM compared to the Eurocode, which tends to be more conservative.

5.10 SHEAR CAPACITY REDUCTION FACTOR COMPARISON PLOT FOR FEM AND DSM AND EURO CODE WITH PERFORATION

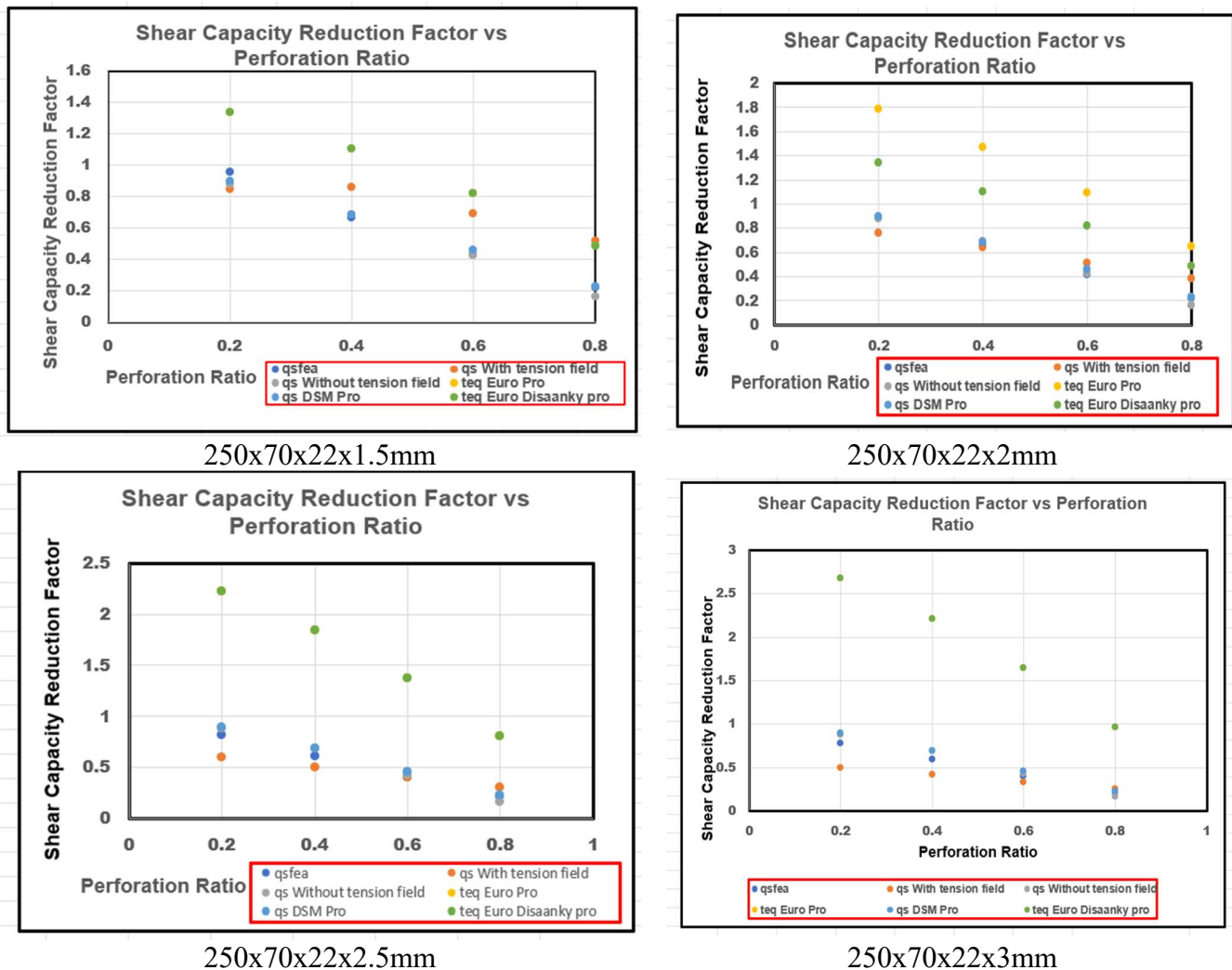


Figure 11 Shear Capacity Reduction Factor Comparison for different Stainless Steel Lipped Channel Beam

Figure 11 presents four graphs illustrating the relationship between the shear capacity reduction factor (qs) and the perforation ratio (d_{wh}/d_1) for different sizes of lipped channel beams, namely 250x70x22x1.5mm, 250x70x22x2mm, 250x70x22x2.5mm, and 250x70x22x3mm. Each graph compares how the shear capacity changes with varying

perforation ratios, showing data points that represent different web depths or boundary conditions. The x-axis denotes the perforation ratio, while the y-axis indicates the shear capacity reduction factor. A clear decreasing trend is observed in all graphs, demonstrating that as the perforation ratio increases, the shear capacity reduction factor decreases, implying that larger web openings cause a greater reduction in shear strength. Furthermore, thicker sections (2.5 mm and 3 mm) exhibit comparatively higher q_s values, indicating better shear resistance than thinner sections (1.5 mm and 2 mm). Overall, the plots highlight that both perforation size and section thickness significantly influence the shear performance of lipped channel beams, emphasizing the need for modified design equations to accurately predict shear capacity in perforated members.

6. CONCLUSION

This study provided a comprehensive numerical and theoretical assessment of the shear behaviour of cold-formed stainless steel lipped channel beams (LCBs) with varying web perforation ratios. The nonlinear finite element analysis, which included 100 models with different web depths, thicknesses, and perforation configurations, demonstrated that shear capacity is highly sensitive to changes in perforation geometry. As the perforation ratio increased, the beams exhibited a progressive reduction in shear strength, with a pronounced drop beyond a ratio of 0.6 due to the substantial loss of effective web area and stiffness. Sections with smaller openings retained partial tension field action, whereas thicker beams consistently exhibited enhanced shear resistance, confirming the combined influence of web geometry and material thickness on structural performance.

The comparative evaluation against existing design provisions revealed that current DSM and Eurocode formulations tend to be unconservative for perforated stainless steel LCBs. These standards do not adequately capture the effects of perforation-induced stress redistribution, nonlinear material behaviour, and post-buckling resistance. The study proposed improved DSM-based and Eurocode-based equations incorporating an equivalent web thickness (t_{eq}) and a modified shear buckling factor (χ_w). These refinements significantly enhanced prediction accuracy, producing strength ratios close to unity and ensuring consistent reliability across all tested sections.

Overall, the findings confirm that the proposed design equations offer a robust, rational, and practically applicable framework for predicting the shear strength of cold-formed stainless steel LCBs with web perforations. By effectively accounting for geometric discontinuities,

nonlinearities, and tension field contributions, the modified models provide safer and more economical design guidance. This work contributes to advancing modern stainless steel design practices and supports the development of more efficient perforated structural systems in engineering applications.

Acknowledgement

We also acknowledge our institution for providing the necessary facilities and academic support for the successful completion of this work.

Conflict of Interests Statement

The authors declare that they have no known competing financial interests or personal relationships that could have appeared to influence the work reported in this paper.

Ethical Approval

This article does not contain any experimental studies with animals performed by any of the authors

Data Availability Statement

The data that support the findings of this study are available from the corresponding author upon reasonable request. Some data, models, or code generated or used during the study are proprietary or confidential in nature and may only be provided with restrictions.

Authors Contribution

PA: Conceptualization, Methodology, Investigation Writing - original draft.

CM: review and editing.

7. REFERENCE

- [1] Vadivelu, P., 2025, *Flexural behaviour of perforated rectangular hollow section beams*, Thin-Walled Structures, 220, 108434.
- [2] Huangfu, S., Zhang, Y. and Li, W., 2025, *Folded-flange and V-stiffened C-shaped stainless steel beams under bending*, Journal of Constructional Steel Research, 213, 108086.
- [3] Jiao, H., 2025, *Shear resistance of stainless steel I-section beams: Experimental and FE investigation*, Journal of Constructional Steel Research, 211, 108065.
- [4] Ivković, I., Djuric, N. and Jovanović, B., 2024, *Application of artificial neural networks for predicting mechanical properties of stainless steels*, Materials Today Communications, 38, 107434.
- [5] Perampalam, P., Dissanayake, P. and Mahendran, M., 2024, *Cold-formed stainless steel lipped channel sections with circular web holes: Experimental and FE studies*, Journal of Constructional Steel Research, 214, 108097.
- [6] Simwanda, M. and Tsavdaridis, K.D., 2024, *Machine learning-based prediction of bending capacity in perforated cold-formed steel beams*, Engineering Structures, 298, 116687.
- [7] Vu, T., Pham, C.H. and Keerthan, P., 2024, *Review on cold-formed steel members with perforations*, Thin-Walled Structures, 197, 110575.
- [8] Amani, M., Li, Y. and Zhao, X., 2023, *Shear behaviour of stainless steel girders with corrugated webs*, Journal of Constructional Steel Research, 193, 108086.
- [9] Real, E., Sánchez, J. and Gardner, L., 2023, *Experimental and numerical investigation on shear response of stainless steel plate girders*, Thin-Walled Structures, 188, 110970.
- [10] Zhou, F., Chen, B. and Zhao, X., 2023, *Shear buckling and ultimate strength of stainless steel girders with circular perforations*, Thin-Walled Structures, 188, 110942.
- [11] Gatheeshgar, P., Bock, M., & Chandrasiri, D. (2023). Assessment of Eurocode shear design provisions for cold-formed steel sections. *Structures*, 47, 2066–2073.
- [12] Yousefi, A. M., Samali, B., & Yu, Y. (2023). Localised Web Bearing Behaviour of Cold-Formed Austenitic Stainless-Steel Channels: Review of Design Rules and New Insight under Interior Loading. *Applied Sciences*, 13(19), 10696.
- [13] Degtyarev, V. and Tsavdaridis, K.D., 2022, *Machine learning prediction of buckling loads of cellular steel beams*, Journal of Constructional Steel Research, 194, 107368.
- [14] Li, H., Ma, Z. and Gardner, L., 2022, *Experimental and numerical studies on stainless steel plate girders with circular web openings*, Thin-Walled Structures, 180, 109478.
- [15] Mangattil, A.L. and Divya, K.K., 2022, *Shear characteristics of perforated lean duplex stainless steel rectangular hollow beams*, IJRASET Journal for Research in Applied Science & Engineering Technology, 10, No. 7.
- [16] Dassanayake, P., Keerthan, P. and Mahendran, M., 2021, *Bending-shear interaction of cold-formed stainless steel lipped channels*, Journal of Structural Engineering, 147, No. 9, 04021120.

- [17] Ishqy, M. F. M., Wanniarachchi, S., Poologanathan, K., Gunalan, S., Gatheeshgar, P., Suntharalingam, T., & Navaratnam, S. (2021). Shear behaviour of cold-formed stainless-steel beams with web openings: Numerical studies. *Structures*, 31, 127–144.
- [18] Yousefi, A. M., Samali, B., & Yu, Y. (2021). Shear behaviour and design of cold-formed ferritic stainless steel channels with circular web openings. *Structures*, 33, 4162–4175.
- [19] De'nan, M.S., Zain, M.F.M. and Nordin, N.A., 2021, *Shear buckling of cold-formed channels with circular and diamond perforations using FE simulations*, *Thin-Walled Structures*, 164, 107809.
- [20] Kweon, J., 2021, *True stress-strain behaviour of 304 and 316 stainless steels*, *Journal of Materials Engineering and Performance*, 30, No. 8, pp. 5921–5932.
- [21] Mohammed, A., & Cashell, K. A. (2021). Structural Behaviour and Fire Design of Duplex and Ferritic Stainless Steel CHS Stub Columns. *International Journal of Steel Structures*, 21, 1280–1291.
- [22] Chen, J., Rossi, B., Real, E. and Gardner, L., 2020, *Experimental and numerical studies on stainless steel plate girders under combined bending and shear*, *Engineering Structures*, 207, 110229.
- [23] Dassanayake, P., Keerthan, P. and Mahendran, M., 2020, *Shear behaviour of cold-formed stainless steel lipped channel beams*, *Thin-Walled Structures*, 157, 107063.
- [24] Laim, L., Rodrigues, J.P.C. and Silva, L.S., 2020, *Flexural-torsional behaviour of cold-formed stainless steel channels*, *Thin-Walled Structures*, 157, 107075.
- [25] Keerthan, P., Dissanayake, P. and Mahendran, M., 2019, *Shear capacity of cold-formed stainless steel lipped channel beams with elliptical web openings*, *Thin-Walled Structures*, 144, 106364.
- [26] Roy, K. and Lim, J.B.P., 2019, *Built-up stainless steel channels under compression*, *Thin-Walled Structures*, 145, 106372.
- [27] Chen, X., Yuan, H., Du, X., Zhao, Y. and Ye, J., 2018, *Shear buckling behaviour of welded stainless steel plate girders with transverse stiffeners*, *Thin-Walled Structures*, 122, pp. 529–544.
- [28] Divya, S. and Keerthan, P., 2018, *Finite element modelling of cold-formed steel beams with perforated webs under shear*, *International Journal of Steel Structures*, 18, No. 5, pp. 1456–1469.
- [29] Tiwari, N., Singh, R. and Kumar, V., 2018, *Effect of recycled bottom ash and coir fibres on stabilization of expansive soils*, *Construction and Building Materials*, 175, pp. 591–604.
- [30] Nilakanmani, M., & Anbarasu, M. (2018). Investigation on Behaviour of Cold-Formed Ferritic Stainless Steel Hollow Beams. *The Asian Review of Civil Engineering*.
- [31] Standards Australia/Standards New Zealand, 2018, *AS/NZS 4600: Cold-formed steel structures*, Sydney/Wellington.
- [32] Jing, L. and Rasmussen, K.J.R., 2017, *Shear buckling and post-buckling of cold-formed stainless steel girders*, *Thin-Walled Structures*, 120, pp. 234–246.

- [33] Pham, C.H., Hancock, G.J. and Rasmussen, K.J.R., 2016, *Shear tests of cold-formed C-sections with central square holes*, Journal of Structural Engineering, 142, No. 5, 04016006.
- [34] Arrayago, I., Real, E. and Gardner, L., 2015, *Stress-strain behaviour of stainless steels at austenitic, ferritic, and duplex grades*, Journal of Constructional Steel Research, 114, pp. 37–49.
- [35] Keerthan, P. and Mahendran, M., 2015, *Shear strength behaviour of cold-formed steel lipped channel beams under pure shear*, Journal of Structural Engineering, 141, No. 11, 04015047.
- [36] Lawson, R. M., Basta, A., & Uzzaman, A. (2015). Design of stainless steel sections with circular openings in shear. Journal of Constructional Steel Research, 112, 228–241.
- [37] N. Baddoo, P. Francis, "Development of design rules in the AISC Design Guide for structural stainless steel", Thin-Walled Structures 83 (2014) 200-208
- [38] Cashell, K. A., & Baddoo, N. R. (2014). Ferritic stainless steels in structural applications. Thin-Walled Structures, 83, 169–181
- [39] Keerthan, P. and Divya, S., 2008, *Shear behaviour of LiteSteel beams*, Journal of Constructional Steel Research, 64, No. 11, pp. 1187–1195.
- [40] European Committee for Standardization (CEN), 2006, EN 1993-1-4: Eurocode 3 – Design of steel structures – Part 1-4: General rules – Supplementary rules for stainless steels, Brussels.
- [41] Schafer, B. W., & Ádány, S. (2006). *Buckling analysis of cold-formed steel members using CUFSM: Conventional and constrained finite strip methods*. Eighteenth Int. Specialty Conf. on Cold-Formed Steel Structures.
- [42] Dassault Systèmes. (2024). *Abaqus 2024 Analysis User's Guide*. Providence, RI: Dassault Systèmes Simulia Corp.